Article

Scenario-Based Uncertainty Modeling for Power Management in Islanded Microgrid Using the Mixed-Integer Distributed Ant Colony Optimization

Maen Z. Kreishan 🆔 **and Ahmed F. Zobaa** *🆔

Electronic and Electrical Engineering Department, Brunel University London, Uxbridge UB8 3PH, UK;
maen.kreishan@brunel.ac.uk
* Correspondence: azobaa@ieee.org

Abstract: Reliable droop-controlled islanded microgrids are necessary to expand coverage and maximize renewables potential. Nonetheless, due to uncertainties surrounding renewable generation and load forecast, substantial power mismatch is expected at off-peak hours. Existing energy management systems such as storage and demand response are not equipped to handle a large power mismatch. Hence, utilizing dump loads to consume excess power is a promising solution to keep frequency and voltage within permissible limits during low-load hours. Considering the uncertainty in wind generation and demand forecast during off-peak hours, the dump load allocation problem was modeled within a scenario-based stochastic framework. The multi-objective optimization with uncertainty was formulated to minimize total microgrid cost, maximum voltage error, frequency deviation, and total energy loss. The mixed-integer distributed ant colony optimization was utilized in a massive parallelization framework for the first time in microgrids to solve the decomposed deterministic problem of the most probable scenarios. Moreover, a flexible and robust load-flow method called general backward/forward sweep was used to obtain the load-flow solution. The optimization problem was applied to the IEEE 69-bus and 118-bus systems. Furthermore, a cost benefit analysis was provided to highlight the proposed method's advantage over battery-based power management solutions. Lastly, the obtained results further demonstrate the fundamental role of dump load as power management solution while minimizing costs and energy losses.

Keywords: ant colony optimization; droop control; dump load; load flow; multi-objective optimization; islanded microgrid; scenario-based stochastic modeling; wind power uncertainty

1. Introduction

Over the last two decades, a major shift from conventional forms of power generation toward renewable energy sources (RES) has occurred to minimize greenhouse gas emissions and facilitate the growth of greener and decentralized electricity supply industry [1]. Likewise, developments in distributed generation (DG) technology, energy conversion efficiency, government incentive programs, and overall cost reductions have given rise to microgrids (MGs) as a viable solution for future smart grid projects [2]. Nonetheless, there are economic and technical challenges that hinder the expansion of islanded MGs (IMGs) which have high RES penetration. The nature of these challenges is associated with the uncertainties surrounding variable renewable generation and demand forecast errors. Conversely, the inability to always match generation with demand, the insufficient transmission capacity to accommodate excess power generation, storage facilities' higher costs, and the need to minimize reliance on fossil fuels are considered the main obstacles that implicate the optimal operation and control of future IMGs [2].

Adequate control of IMGs is necessitated by international standards, such as IEEE Std. 1547, to maintain voltage and frequency $(V - f)$ within acceptable margins [3]. Moreover, a reliable control strategy is fundamental to ensure the autonomous participation of all DGs

to cover any variations in demand. Therefore, droop control is often selected to enable the autonomous sharing of loads within an IMG due to its higher reliability and lower costs compared to other control schemes [4]. As a result, IMGs that adopt the latter strategy are referred to as droop-controlled IMGs (DCIMGs). Conversely, with RES penetration levels exceeding 10% in emerging MGs, one major issue remains is how to relieve network congestion and grid integration difficulties. Hence, alleviating such issues arising from large power mismatches in DCIMGs shall maintain $V-f$ safe limits [5]. There are several energy management systems (EMS) that handle power deviation problems in DCIMGs. Such EMS include energy storage systems (ESSs) [6], demand response programs [7], and electric vehicle smart charging [8]. Nevertheless, electric vehicle and demand response programs are often challenging to coordinate and execute [9], while battery ESSs (BESSs) suffer from high standing losses, environmental degradation, and expensive transportation costs [10]. Therefore, EMS strategies that are based on electric vehicles and ESSs are suitable to manage small power mismatches during peak hours as a secondary solution, while different arrangements should be sought for at the event of prolonged wind generation exceeding two load cycles.

Dump loads (DLs) are considered as a good solution to absorb excess power to provide $V-f$ support for synchronous and asynchronous generators [11,12]. Moreover, the use of DL as dissipated heat with the help of an electronic load controller (ELC) has been utilized for hydro and wind self-excited induction generators [13,14]. Conversely, DLs were put into heating and pumping applications to handle $V-f$ deviations of the system [15,16] while DL application was distributed as an experimental multi-ELC project to provide hot water and heating services for households in a micro-hydro-driven MG [17]. However, DLs are considered preliminary when it comes to power management solutions for DCIMGs; that is, studies seeking DL optimization within an IMG framework are scant. On the other hand, various attempts were made to find the optimal location and size of DG and ESS units serving various technical and economic objectives [18–21]. Nevertheless, studies [18–21] did not account for $V-f$ deviations at low load hours, nor did they consider generation and demand uncertainties.

To accommodate uncertainties in wind power and demand forecast errors within an EMS solution, the optimal droop settings of DGs were optimized in [22] to maximize loadability and minimize fuel costs. Likewise, the total MG cost was minimized in a real-time EMS as a stochastic solution considering demand response and BESS limits [23]. Conversely, the authors of the stochastic EMS solution in [24] have sought emission reductions as a stand-alone objective alongside cost minimization while taking BESS as a backup to the IMG. Moreover, the work in [25] has taken similar approach as [24] by optimizing the droop setting of dispatchable DGs but with loadability maximization as an additional objective. In spite of the advancements in the uncertain EMS studies of [22–25], they did not provide a viable solution to the reliability issues of BESS as an off-peak primary management solution. Furthermore, the works in [22–25] did not account for the expected high generation/demand mismatch at low-load hours. Consequently, a novel attempt was made in [26] by allocating a DL to eliminate $V-f$ deviations during off-peak hours. Thus, providing a legitimate solution to the efficiency problems of BESS- and demand-response-based EMS. Furthermore, the single DL allocation given in [26] was extended in [27] to allocate multi-DL units across a DCIMG to minimize the same objectives. Nonetheless, the DL problems provided by [26,27] have failed to address MG operational costs, emissions, and losses expected from DL allocation. Likewise, the work in [26–28] neither distinguished between dispatchable and non-dispatchable units nor considered uncertainties associated with wind and load powers.

Uncertainty in DCIMG operation roots back to the random parameters that define renewable energy and load diurnal state. The DL allocation into DCIMG is considered as a many-objective non-convex mixed-integer nonlinear programming (MINLP) problem. Moreover, by adding the uncertain non-decision variables into the optimization problem (i.e., wind and load uncertain powers), then the optimization problem is changed from a

deterministic optimization problem with certain dimensions to become stochastic optimization problem with random boundaries. To that end, any chosen optimization technique must be able to accurately handle a significant batch of objective function evaluations within a reasonably small calculation time. This is considered fundamental to facilitate real-time EMS solutions within the smallest load cycles possible. Inversely, many of those stochastic EMS solutions [22–25], have neglected the enormous calculation time that will certainly render such solutions not fit for load cycles of less than 10 min. Ant colony optimization (ACO) is an acclaimed metaheuristic for a variety of engineering problems [29,30]. However, the proposed optimization technique, mixed-integer distributed ACO (MIDACO), is based on the extension of ACO into the mixed-integer domains known as mixed-integer ACO (ACOmi) [31] collated with a robust penalty method known as the oracle penalty method (OPM) [32]. The multi-objective handling by MIDACO is based on the utopia–nadir balance approach which aims to locate the best point on a Pareto front. Additionally, a massive parallelization strategy is utilized by fine-grained or co-evaluation parallelization to enable thousands of function evaluations in the shortest times possible [33,34]. The main two significant advantages of MIDACO are its high-speed and accurate computational abilities. Thus, MIDACO is regarded as the state of the art in evolutionary and swarm intelligence computation for many-objective problems [33,35,36].

Due to the foregoing, it was deduced that ESS- and demand-response-based EMS strategies are not suitable to manage high power mismatch at off-peak hours. Moreover, neglecting uncertainty in wind power and load forecast has a negative impact on future DCIMG planning and optimal set-points. Previous DL studies as a power management solution during low demand hours [26–28], albeit scarce, have overlooked fundamental facets of the problem formulation in terms of adequate uncertainty modeling, MG running costs, DG emissions, and total energy losses. In this article, a novel methodology has been proposed to tackle shortfalls in previous studies by formulating a multi-objective stochastic optimization problem across the off-peak hours' horizon. Four objectives were minimized in total, viz., the expected total microgrid cost (TMC), the expected maximum voltage error (MVE), the expected frequency deviation, and the expected total energy loss (TEL). This was done using a state-of-the-art technique, MIDACO, combined with a newly developed and robust load-flow method. The stochastic optimization problem for optimal DL allocation and DG droop selection was modeled on IEEE 69-bus and 118-bus systems. So far and to the best of the authors' knowledge, no previous work has addressed the uncertainty in generation and demand during off-peaks hours within a DCIMG framework. Furthermore, all DCIMG optimization studies heretofore have neglected the impact of uncertainty during low-demand hours and their calculation burden. A summary of the main contributions of this work is as follows:

- The DL allocation problem was tackled for the first time as a stochastic optimization problem within a scenario-based uncertainty framework.
- A roulette wheel mechanism was utilized to generate 10,000 scenarios for generation and demand imbalance rather than a set of a few highly probable deterministic mismatch scenarios, as in [28].
- The DL allocation problem was tackled considering technical, environmental, and economic objectives to provide comprehensive outlook on the optimal IMG operation during off-peak hours.
- A robust, adaptive, and derivative-free method, the general backward/forward sweep (GBFS), was used to provide load-flow solution. GBFS offers more accurate representation of DG power updates compared to the load-flow method in [28].
- The proposed optimization technique, MIDACO, has been utilized for first time in a stochastic optimization with uncertainty in microgrids. The proposed technique offers a massive parallelization framework to handle the calculation burden of uncertainties. Furthermore, it offers competitive selection criteria for the non-dominated solution compared to other acclaimed metaheuristics.

- The advantage of DL-based EMS against battery-based EMS is further demonstrated via cost benefit analysis to provide yearly hot water demand for the microgrid.

This article is organized as follows: in Section 1, a brief introduction to the DL allocation problem in DCIMG with uncertainty in generation and demand. In Section 2, the methodology of droop control, uncertainty modeling, the proposed optimization method, and the proposed load-flow technique are described. In Section 3, the stochastic optimization problem is illustrated. Lastly, in Sections 4 and 5, a thorough discussion of the results and conclusions are presented, respectively. Additionally, to enhance the readability of this article, lists of all acronyms and symbols used herein are given in Tables A1 and A2, respectively, in Appendix A.

2. Methodology

In this section, the complete methodology for droop control, scenario-based uncertainty, optimization method, and load-flow technique as proposed in this article are elaborated in more detail.

2.1. Droop Control and Dump-Load-Based Energy Management System

The majority of DG units within IMG are interfaced as voltage source converters with bidirectional power flow where power electronics enable autonomous power sharing capability by droop control [4]. To that end, active and reactive powers are shared by means of active power–frequency ($P - f$) and reactive power–voltage ($Q - V$) droop relationships, respectively. For an inverter-based DG (IBDG) with inductive output impedance, the $P - f$ and $Q - V$ droop relations are given mathematically as in Equations (1) and (2) [28]:

$$f - f_0 = m_{pi}(P_{Gi} - P_{Gi0}),\tag{1}$$

$$|V_i| - |V_0| = n_{qi}(Q_{Gi} - Q_{Gi0})\tag{2}$$

where $|V_0|$ and $|V_i|$ are the reference and operational voltage at bus i, respectively. Q_{Gi0} and Q_{Gi} are the reference and generated reactive power at bus i, respectively. f_0 and f are the IMG reference and operational frequency, respectively. P_{Gi0} and P_{Gi} are the reference and generated active power at bus i, respectively. m_{pi} and n_{qi} are the active and reactive droop coefficients at bus i, respectively.

Moreover, the instantaneous droop control action of IBDG forms the foundation of an IMG hierarchal control strategy. The hierarchal control consists of three levels, viz., primary-level, secondary-level, and tertiary-level control. The primary level is achieved within a matter of seconds in response to the variation in load by the action of IBDG droop control. The secondary control, on the other hand, dictates the recovery of voltage and frequency to their nominal values. That is achieved by vertically shifting the curves of $P - f$ and $Q - V$ upwards or downwards depending on the under- or over-generation responses, respectively, by the primary control. The $P - f$ and $Q - V$ curves of an IBDG are depicted in Figure 1.
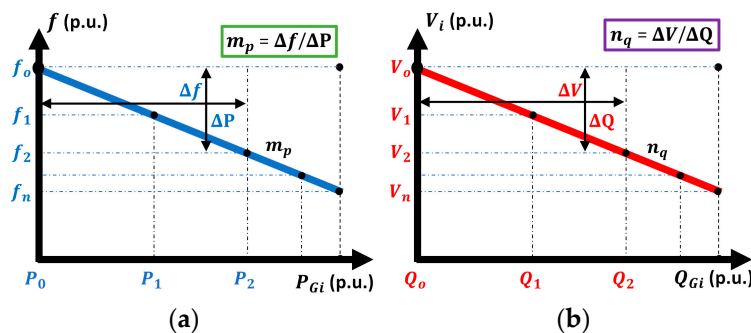

Figure 1. IBDG droop control relations: (a) $P - f$ (b) $Q - V$.

Lastly, tertiary control is dictated by the presences of an MG central controller (MGCC) [24]. The MGCC is defined as the complete EMS strategy that is responsible for data collection, analysis, and optimization to determine the IMG optimal set-points for the controllable components. The MGCC is responsible for conducting a complete optimal load-flow of the system considering uncertainties during optimization cycles. The frequency of the optimization cycles is determined by the IMG needs and can be undertaken days, hours, or up to 15 min ahead. The shorter the optimization cycle is, the more reliable and accurate the optimal solutions provided by the MGCC are. The forecasted data presented to the MGCC are used to determine the optimal droop values and DL setting for the next IMG operational interval. This is ideally fed to DG and DL using a non-critical and low-bandwidth communication interface. This type of communication channel is only necessary at the end of each optimization cycle, thus increasing the reliability of the system. Likewise, according to the assumed notion of this study, large power mismatch at off-peak hours could not be sorted by relying only on BESS and demand response programs.

Consequently, IMG planning must be done first to optimize DL location, while a real-time DL-based EMS is utilized thereafter to deliver the optimal DG droop sets and DL size by virtue of MGCC. The idea is to balance the system's $V - f$ fluctuations via dumping the extra power [28]. Accordingly, this extra DL power can be applied in pumping and heating applications via electric boilers and water circulation systems. The role of BESS in this EMS strategy—or any other suitable auxiliary power management solution, for that matter—would be to simply manage any light deviation in generation and demand during peak hours. The proposed DL-based EMS of this study is depicted in Figure 2.
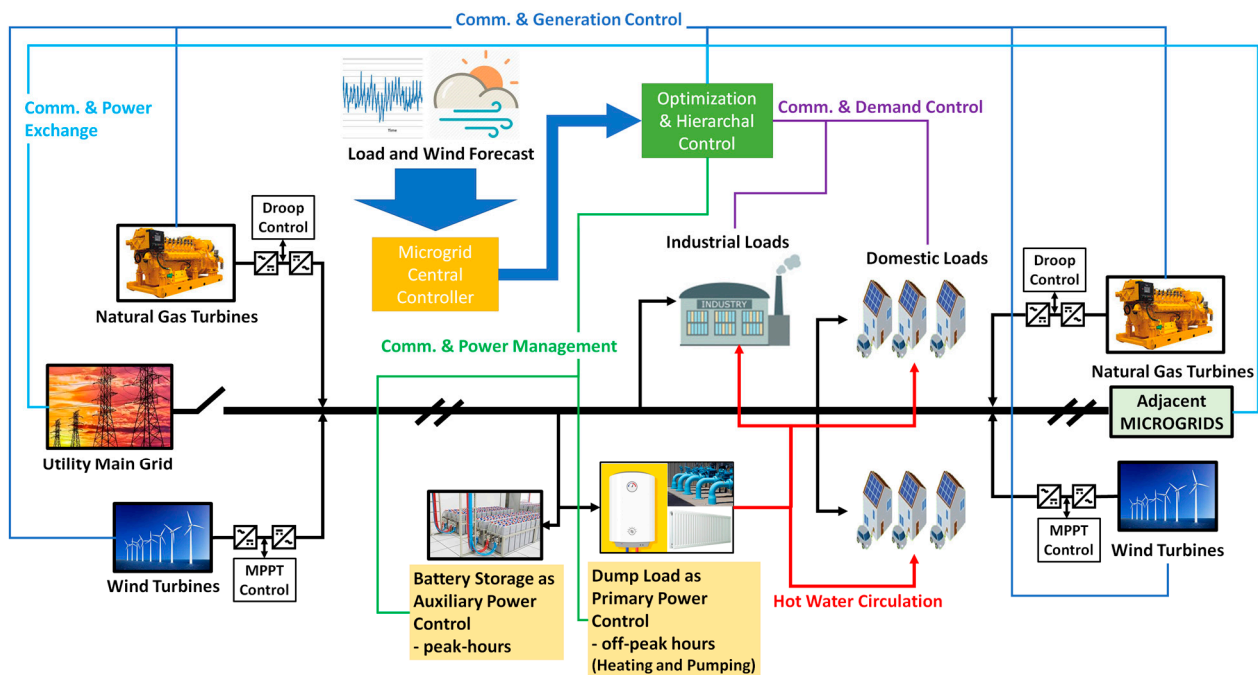

Figure 2. Dump-load-based energy management system.

The load model chosen to represent the loads including the DL in the IMG of this study follows the static load model. According to the literature [37], the static load model is sufficient to describe the static components and approximate the dynamic components of the load. To that end, the constant power model was selected for this study by setting all load coefficients to zero [28].

2.2. Scenario-Based Stochastic Uncertainty Modeling

There are a variety of issues that might affect how definitive a variable is. The majority of these issues are naturally occurring and related to inaccuracies in previous data

collection, forecasting future data, and acquiring data specific to that variable [38]. As a result, the presence of random variables alters the nature of IMG analysis and planning from a deterministic framework with fixed variables to one of a stochastic nature with uncertain variables. To that aim, planning issues for IMG must integrate a suitable uncertainty analysis tool. When it comes to a stochastic framework, probabilistic modeling is the favored option, where each uncertain variable is described as a probability density function (PDF) [2]. These PDFs are used to determine the likelihood that a certain random variable will occur, wherein each PDF is divided into various unique probability levels [38]. There are broadly three main probabilistic methods, viz., Monte Carlo simulation (MCS), analytical methods, and approximation methods [39,40]. MCS methods are very efficient when problem solution search space is limited, while analytical methods are best when the number of random variables is low. Nonetheless, the optimization problem herein contains a huge solution search space with a large number of random variables. Thus, an approximation method is the best trade-off to attain an expected good solution. Out of the available approximation methods, scenario-based analysis is sought after when the number of random variables is large. To increase the accuracy of the method, the number of scenarios must increase, which will lead to higher computational burden. Nevertheless, this issue is eliminated via the proposed optimization technique; MIDACO can handle a large number of many-objective problems with a huge solution search space in a very fast calculation effort via massive parallelization framework [33,34,36].

2.2.1. Stochastic Load and Wind Modeling

Forecasted, historical, and measured load data are all determining factors toward the degree of load uncertainty. The study herein presumes that historical annual load data are available and that the system peak demand conforms with the IEEE reliability test system for load hourly shape [41,42]. Additionally, an hour-by-hour prediction system is used to characterize load uncertainty as a normal-distribution PDF in accordance with standards within the literature [43,44]. Typically, loads are distributed around the mean for any given hour, that is, by considering the load's percentage from the overall system demand in the form of an annual cumulative percentage. Additionally, for this study, a seven-hour window from 12 am to 7 am has been chosen to reflect the off-peak hours scenario with higher accuracy. Thus, normal distribution of each load was segmented into fifteen levels with lengths equal to half the standard deviation from the mean; that is, improved uncertainty modeling with a higher number of levels. Conversely, one of the most significant RESs in the world is regarded as wind energy. However, wind power is mostly dependent on wind speeds and, hence, is intrinsically intermittent in nature, much like many other unstable RESs. Therefore, it is essential to account for the influence of wind speed on wind power through suitable probabilistic uncertainty modeling. Wind speed, however, fits the Weibull distribution PDF rather than the normal distribution PDF of a load's probabilistic model [42,45]. A wind speed (v) represented by a PDF, referred to herein as ϕ_W, with a scale index c_s and shape factor k_s to conform with Weibull distribution is given by [45]:

$$\phi_W(v) = \frac{k_s}{c_s}\left(\frac{v}{c_s}\right)^{k_s-1} e^{-\left(\frac{v}{c_s}\right)^{k_s}}, \tag{3}$$

For a Weibull distribution, k_s and c_s may be calculated in a variety of ways. However, k_s and c_s may be roughly estimated using the following formulas [42,45,46], provided that the average wind speed μ_W and its standard deviation σ_W of a certain site are known.

$$k_s = \left(\frac{\sigma_W}{\mu_W}\right)^{-1.086}, \tag{4}$$

$$c_s = \frac{\mu_W}{\Gamma\left(1 + \frac{1}{k_s}\right)}, \tag{5}$$

where the symbol $\Gamma()$ refers to the gamma function. Detailed information regarding the wind speed PDF as well as k_s ands c_s derivations are found in [46,47]. Nevertheless, as per the assumed notion of this study, the wind speed's mean and standard deviation are known in the form of historical annual data for a typical wind farm covering the previous three years [45]. Additionally, according to the study's presumption, power is always available during peak hours, whereas wind speeds at higher elevations often tend to progressively rise during off-peak hours [48]. Subsequently, a PDF for wind speed is also discretized into several levels or states, where each level reflects a range of projected wind speeds. To achieve high accuracy for wind speed stochastic modeling, a 30 wind levels/states were constructed from zero wind speed increasing by a 1 m/s increment. Therefore, the probability of any given wind state (W_{st}) is equal to:

$$\Lambda(W_{st}) = \int_{v_{st}^l}^{v_{st}^u} \phi_W(v)dv, \tag{6}$$

where v_{st}^u and v_{st}^l are the upper and lower limits of wind speed for state W_{st}. For a typical wind turbine (WT), the output power ($P_W(v_{st})$) as a function of the mean wind speed (v_{st}) during the state (W_{st}) is given by [42,45]:

$$P_W(v_{st}) = \begin{cases} 0, & v_{st} < v_{ci} \ or \ v_{st} \geq v_{co} \\ P_{Wr}\left(\frac{v_\mu - v_{ci}}{v_r - v_{ci}}\right), & v_{ci} \leq v_{st} < v_r \\ P_{Wr}, & v_r \leq v_{st} < v_{co} \end{cases}, \tag{7}$$

$$v_{st} = \frac{v_{st}^u + v_{st}^l}{2}, \tag{8}$$

where P_{Wr} is the WT rated power. v_{co} and v_{ci} are the cut-off and cut-in wind speeds, respectively, with the former also known as the furling wind speed. v_μ is the site's average wind speed. v_r is the WT rated wind speed.

2.2.2. Scenario Generation, Reduction, and Aggregation

A sizable number of wind and load states is created as potential scenarios based on wind speed and load forecast PDFs. Moreover, by considering a roulette wheel mechanism (RWM) for this study, each unique PDF will be linked to a separate RWM. Subsequently, 10,000 scenarios are generated, where each (s) scenario is defined by the set (Ω_s) of uncertain variables. As a result, each Ω_s consists of the values for each wind and load power random variable as well as their relative probability (Λ_s^i). Likewise, the set Ω_s is defined in an IMG for an $\mathcal{N}$ number of buses as:

$$\Omega_s = \left\{ P_{L1}^s, \ldots, P_{Li,lk}^s, Q_{L1}^s, \ldots, Q_{Li,lk}^s, P_{W1}^s, \ldots, P_{Wi,wk}^s \right\}, \forall i \in \mathcal{N}, \tag{9}$$

$$NV = 2lk + wk, \tag{10}$$

where P_{Wi}^s, P_{Li}^s, and Q_{Li}^s are the WT, load active, and load reactive powers at bus i during scenario s, respectively. NV is the number of uncertain variables in scenario s. lk and wk are the total number of loads and WT in the network, respectively. Each RWM is fragmented into many slots equal to the number of probability levels of the PDF, whereas an RWM slot length is defined by the random variable's corresponding normalized probability [24,38]. Each uncertain variable is obtained from the RWM tool using a random number between 0 and 1. That is, an RWM slot is selected depending on the generated random number and its location on the RWM tool. Subsequently, the uncertain variable tagged with that slot along with its associated normalized probability are chosen. To attain the required number of scenarios, the slots selection process is repeated for all uncertain variables and for every s scenario. Nonetheless, many of the 10,000 created scenarios will have low probability and thus no bearing on the solution. As a result, eliminating repeated

and low-probability scenarios must take place by selecting fewer and dissimilar scenarios with the highest probabilities. A reduced number of scenarios (NR) for this work was selected as 20 to conform with current norms in uncertainty modeling techniques [24,49]. Lastly, each of the NR scenarios of the stochastic planning problem may then be utilized to construct a separate deterministic optimization problem. As a result, the probability of each deterministic problem's optimal solution within a scenario s will be equal to the convolved probability of all uncertain variables [50]. It is important to note that this study makes the premise that the events linked to wind speed and load forecast are uncorrelated [42]. In other words, neither the occurrence of a certain load state nor the occurrence of a particular wind speed state is affected by the other. This presumption is consistent with the notion herein that holds that generation will almost certainly be higher than demand during off-peak hours. Therefore, for a scenario s, the convolved normalized probability Λ_s^N is obtained by:

$$\Lambda_s^N = \frac{\prod_{i=1}^{NV} \Lambda_s^i}{\sum_{s=1}^{NR} \prod_{i=1}^{NV} \Lambda_s^i},$$ (11)

Additionally, for each s scenario's deterministic problem, an aggregation technique based on weighted sum is used; that is, by accumulating the optimal solutions considering the importance of each scenario based on its higher probability effect. Thereby, the expected value for the objective function ($\check{\mathscr{F}}_\imath(x)$) of the stochastic problem taking into account all NR scenarios is provided by [38,49]:

$$\check{\mathscr{F}}_\imath(x) = \sum_{s=1}^{NR} \mathscr{F}_\imath^s(x) \cdot \Lambda_s^N$$ (12)

2.3. The Proposed Optimization Algorithm

As mentioned in the introduction, the proposed DL stochastic optimization problem is a many-objective non-convex MINLP. This implies that the solution search space is challenging and vast. Such problems are known not to have a solution in polynomial time, making deterministic solvers inapplicable. Hence, to solve the stochastic many-objectives problem, a state-of-the-art metaheuristic algorithm, MIDACO, is proposed herein. This evolutionary algorithm is considered as an advanced hybrid optimization technique. It employs different heuristics for better exploration and a back-tracking local deterministic solver for enhanced exploitation [33]. The main components of the MIDACO algorithm are the ACOmi for constructing iterates, or ants, using PDFs and the OPM for evaluating penalties from constraint violations [33]. By employing the extended ACO for mixed-integer domains, the proposed method relies on a multi-kernel Gaussian PDF to construct solutions instead of a pheromone table as in the primordial ACO. For single-objective MINLP handling by MIDACO, three parameters are very influential, viz., ANTS, KERNEL, and ORACLE [33]. That is, for constructing solutions, the method starts with a dynamic population of ants (N_{pop}) within a (k_r) number of kernels to generate and fine-tune ants as they get evaluated according to their oracle penalty value [31]. A user-desired value for the objective function known as the oracle (Ω) estimates the penalty function value within OPM [32]. Conversely, for multi-objective MINLPs, MIDACO uses the utopia–nadir balance concept to decompose the original problem into a series of single-objective sub-problems, each solved in the $\imath$-th dimension [51]. This approach explores the Pareto front much faster and more efficiently leading to a better convergence of the multi-objective optimization. This differs from a non-dominated sorting approach that gives the entire Pareto front an equal importance making convergence much slower [33,51]. Another advantage for the utopia–nadir balance approach is that, eventually, the best equally balanced solution is selected [33,51]. Thus, an additional multi-criteria decision approach is not required in MIDACO. Accordingly, for any mixed-integer solution x that belongs to set of feasible solutions $\mathbb{F}$, the utopia ($U_\imath$) indicates the fittest overall value for an objective function $\mathscr{F}_\imath(x)$

whereas a nadir (N_i) is by far the least fit $\mathscr{F}_i(x)$ value that relates to different utopia as follows [51]:

$$U_i = min\{\mathscr{F}_i(x) \forall x \in \mathbb{F}\}, \tag{13}$$

$$N_i = max\{\mathscr{F}_i(x) \,\forall\, x : \exists\, k \neq i : \mathscr{F}_k(x) = U_k\}, \tag{14}$$

Once the utopia–nadir information is known, then the solution x weighted $d_i^j(x)$ and average $D_j(x)$ distances are calculated for an M-objectives MINLP. This is done for each objective i within the j-th dimension as follows [51]:

$$d_i^j(x) = w_i^j \cdot \left(\frac{\mathscr{F}_i(x) - U_i}{N_i - U_i} \right), \tag{15}$$

$$D_j(x) = \frac{\sum\limits_{i=1}^{M} d_i^j(x)}{M}, \tag{16}$$

Subsequently, by having $d_i^j(x)$ and $D_j(x)$ for each sub-problem as well as the utopia–nadir information, a scalar function known as the balance function is created [51]:

$$B_j(x) = \sum_{i=1}^{M} \left| d_i^j(x) - D_j(x) \right|, \tag{17}$$

Each j-th sub-problem is solved as a single-objective problem using the target function $T_j(x)$ as defined hereafter [51]:

$$T_j(x) = \sum_{i=1}^{M} d_i^j(x) + B_j(x), \tag{18}$$

Eventually, the original problem is re-constructed again using the set of target functions $\{T_1, T_2, \ldots, T_M\}$ evaluated in series or in parallel to attain the Pareto front. For CPU-time-intensive problems, such as the stochastic one proposed in this article, MIDACO offers a very efficient parallelization strategy. This strategy, known as fine-grained parallelization, handles the execution of objective and constraint functions in each individual ACOmi instance in parallel [33]. To fine-tune multi-objective optimization, MIDACO utilizes the parameters, viz., BALANCE, EPSILON, and PARETOMAX. As for the former, it dictates the Pareto front search direction, thus expediting the convergence. The latter two parameters influence the precision and number of Pareto point collection, respectively. Other parameters such SEED and ACCURACY enhance the solution's global optimality and suitability, respectively [33]. The proposed optimization technique flow chart is depicted in Figure 3.

2.4. The Proposed Load-Flow Method

There exist different load-flow techniques such as Gauss–Seidel, Newton–Raphson, and backward/forward sweep (BFS) [28]. Nonetheless, many of them are not well-equipped to provide load-flow for IMG because of the low X/R ratio in distribution systems. Moreover, IMG has a variable system frequency and no constant slack bus voltage. Therefore, a special BFS (SBFS) method was proposed in [28] to account for droop Equations (1) and (2). However, the reactive power update in SBFS does not account for local DG voltage measurements. These local measurements are necessary for IMG with little or weak communication infrastructure. Conversely, GBFS was proposed in [52] which has two main stages, viz., BFS stage and update stage. These will be described briefly as follows.
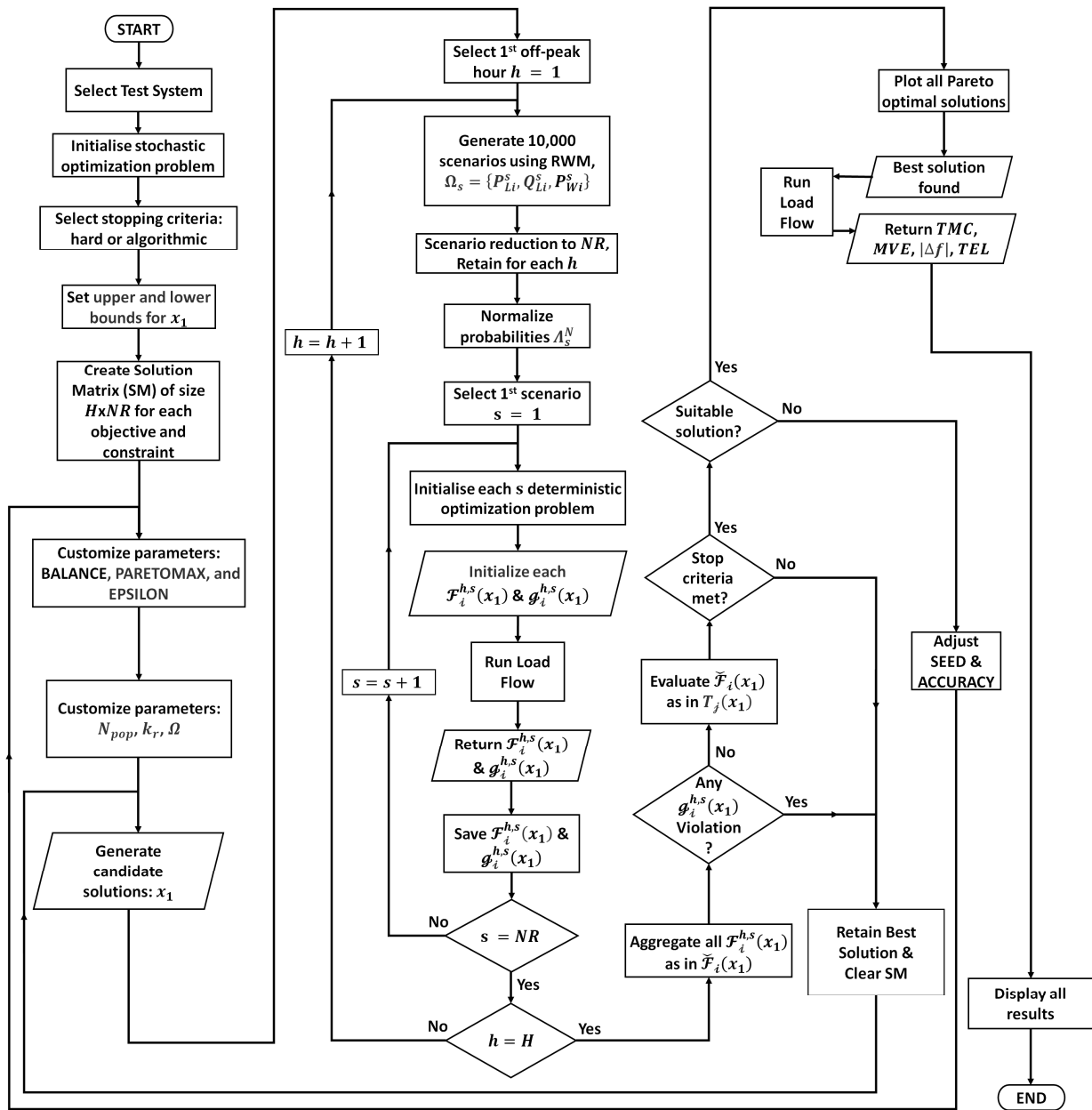
Figure 3. Flow chart of the proposed optimization method to solve the problem of DL allocation with uncertainty.

2.4.1. Backward/Forward Sweep Stage

At this stage, all IMG variables are initialized, and all system quantities are calculated. The value $1 \angle 0°$ p.u. is given to voltages of all system buses including the virtual bus (VB). A VB mimics the behavior of a slack bus in grid-connected load flow; however, it has a variable voltage. Subsequently, inject currents as well as branch currents for all buses are calculated in forward sweep. Inversely, voltages on each system bus, except VB, are obtained in the backward sweep as follows [52]:

$$[I_i] = ([S_i]/[V_i])^*, \tag{19}$$

$$[B_i] = [BIBC][I_i], \tag{20}$$

$$[V_{in}] = [V_1] - [BCBV][B_i], \tag{21}$$

$$V'_{in} = V_{in} - \zeta_1 \cdot (V_{in} - V_i), \tag{22}$$

$$\left| \Delta V'_{in} \right| = \left| V'_{in} - V_{in} \right|, \tag{23}$$

$$\Delta f = -m_{pT} \cdot (P_{G1} - \mathscr{R}\{V_1 \cdot B_1^*\}), \tag{24}$$

$$\Delta V_1 = -n_{qT} \cdot (Q_{G1} - \mathscr{I}\{V_1 \cdot B_1^*\}), \tag{25}$$

where, for a radial system with n buses, $[S_i]$, $[V_i]$, $[I_i]$, and $[B_i]$ are all column vectors of size $n - 1$ by 1 and correspond to at bus i as the apparent power inject, initial bus voltage, current inject, and branch current, respectively. $[BIBC]$ and $[BCBV]$ are matrices of size $n - 1$ by $n - 1$ for branch inject–branch current as given in [53] and branch current–bus voltage as given in [28], respectively. $[V_1]$ and $[V_{in}]$ are column vectors of size $n - 1$ by 1 for VB voltage and new bus voltages, respectively. ζ_1 is the dynamic damping factor to suppress the oscillations in the system voltage error vector $\left| \Delta V'_{in} \right|$ as obtained stochastically by MIDACO in [52]. V'_{in} is the new bus voltage vector as attained using ζ_1 and another sweep for V_i. Δf and ΔV_1 are the system frequency and VB voltage deviations, respectively. P_{G1} and Q_{G1} are VB-generated active and reactive powers, respectively. In the case that the VB has no DG unit connected to it, these values are set to zero. $V_1 \cdot B_1^*$ is the total apparent power exchanged at the VB. m_{pT} and n_{qT} are the system effective active and reactive droop coefficients at VB as defined in [28], and are given by:

$$m_{pT} = \left(\sum_{i \in \mathscr{GK}}^{gk} m_{pi}^{-1} \right)^{-1}, \tag{26}$$

$$n_{qT} = \left(\sum_{i \in \mathscr{GK}}^{gk} n_{qi}^{-1} \right)^{-1}, \tag{27}$$

2.4.2. The Update Stage

In this stage, the VB voltage and system frequency are updated along with the DGs' active and reactive powers as follows:

$$V_{1c+1} = V_{1c} + \zeta_2 \cdot \Delta V_1, \tag{28}$$

$$f_{c+1} = f_c + \Delta f, \tag{29}$$

$$P_{Gi} = \Delta f / m_{pi} + P_{Gi0}; \forall i \in \mathscr{GK}; \mathscr{GK} \subseteq \mathscr{N}, \tag{30}$$

$$Q_{Gi} = (|V_{in}| - |V_0|) / n_{qi} + Q_{Gi0}; \forall i \in \mathscr{GK}, \tag{31}$$

where f_{c+1} and f_c are, respectively, the system frequency at the $c + 1$ and c-th iterations. V_{1c} and V_{1c+1} are, respectively, the VB voltage at the $c + 1$ and c-th iterations. ζ_2 is the dynamic damping factor to suppress the oscillations in the VB voltage error vector $|\Delta V_1|$ as obtained stochastically by MIDACO in [52]. Calculation of ζ_1 and ζ_2 is presented in more detail in the following section. P_{Gi0} and Q_{Gi0} are the active and reactive power reference points at bus i, respectively. $\mathscr{GK}$ and $\mathscr{N}$ are sets for system generating buses and all system buses, respectively. Another distinct feature of GBFS compared to other BFS-based methods such as modified and nested BFS [52] is having one loop. This calculation loop with the counter c helps in minimizing computation burden by eliminating many internal loops. Moreover, according to GBFS implementation, the reactive power update of DG units considers the local voltage at each generating bus to mimic the nominal voltage $|V_0|$ recovery of DG units. However, such an approach will often cause divergence problems for ill-conditioned systems. Such issues are due to IMG with lower droop settings, high generation/demand mismatch, or higher line impedance. As a result, the correction vector for reactive power

was proposed by GBFS in [52] and denoted here as γ_i. The aim of γ_i is to eliminate the reactive power error $|\Delta Q_{Gi}|$ in the IMG.

$$\gamma_i = \left(\frac{Q_c}{\sum_{i \in \mathcal{GK}} |\Delta Q_{Gi}|} - 1 \right) \cdot \{|\Delta Q_{Gi}|\} \cdot \beta, \tag{32}$$

where Q_c is the IMG correction factor based on average reactive power in the IMG, and is provided by [52]:

$$Q_c = -(Q_{G1} - \mathcal{I}\{V_1 \cdot B_1^*\}), \tag{33}$$

Furthermore, to ensure adequate reactive power correction, β, a binary constant, was added to (32) to disable or enable the reactive power correction based on IMG needs [52]:

$$\beta = \begin{cases} 0, & \forall \, Q_{min} < Q_{Gi} < Q_{max} \\ 1, & \forall \, Q_{Gi} \leq Q_{min}, Q_{Gi} \geq Q_{max} \end{cases}, \tag{34}$$

Subsequently, the reactive power reference is adjusted to account for any power limit violations. Thus, a new reactive power value (Q'_{Gi}) is used and given by [52]:

$$Q'_{Gi} = Q_{Gi0} + \gamma_i + |\Delta Q_{Gi}|; \, \forall \, i \in \mathcal{GK}, \tag{35}$$

If $\beta = 0$, this implies γ_i is disabled and no change to reactive power is performed, i.e., $Q'_{Gi} = Q_{Gi}$. In addition, due to frequency update, line impedance (Z_i) is updated.

$$Z_i = R_i + jX_i(f_{c+1}/f_c) \tag{36}$$

where R_i and X_i are the resistance and reactance of the line connecting bus i and $i+1$, respectively. Lastly, GBFS exits the loop when the condition for convergence is satisfied; in other words, by attaining an objective function ($\mathcal{F}(x_0)$) value below the voltage error threshold (ε_{Th}), as will be explained in the next section. That is, GBFS terminates when $\mathcal{F}(x_0) < \varepsilon_{Th}$, noting that $\varepsilon_{Th} = 10^{-8}$ for all investigated cases in this article. A flow chart of GBFS is depicted in Figure 4.
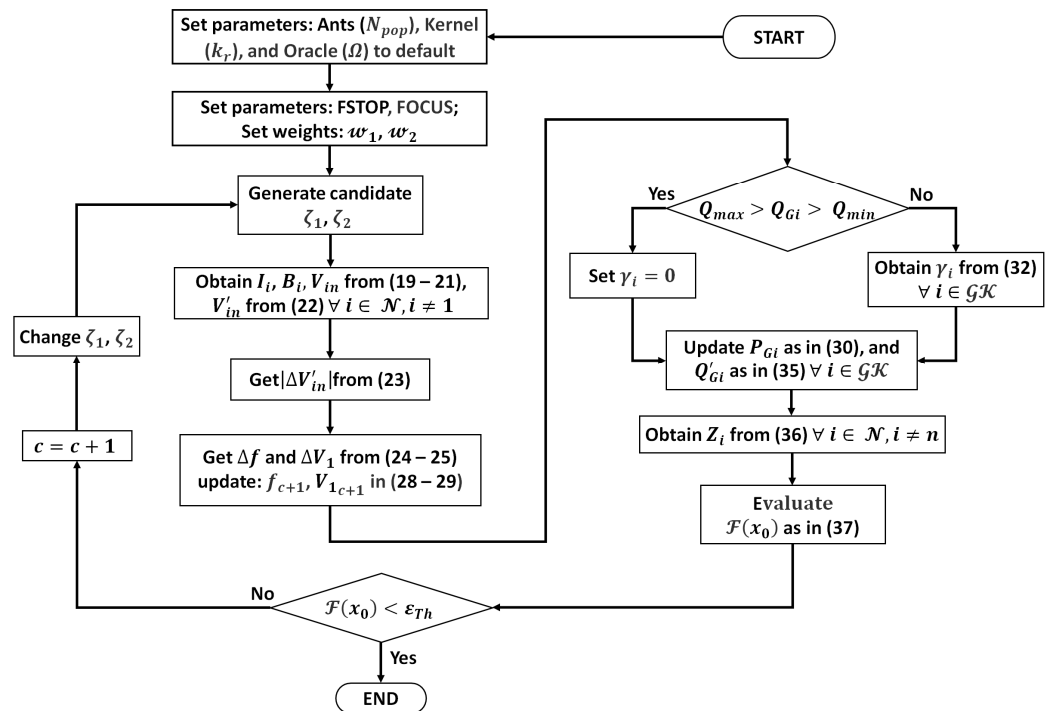

Figure 4. Flow chart of the proposed load-flow method.

3. Optimization Problem Formulation

In this section, the objective functions and constraints for the stochastic DL optimization considering uncertainty in wind and load power are described in detail.

3.1. Objective Function for Dynamic Damping Factors in GBFS

The objective in the optimization problem of GBFS is to obtain a concurrent minimization of the two main voltage error vectors $|\Delta V'_{in}|$ and $|\Delta V_1|$. This is achieved by stochastically adjusting the dynamic damping factors ζ_1 and ζ_2. A weighted sum approach was elected to attain the dynamic adjustment of ζ_1 and ζ_2 without computational overhead and extra run time. This is attributed to weighted sum benefit in simplifying and transforming the multi-objective problem into a single objective [40,54]. Furthermore, due to the existing knowledge of the objective function desired threshold, i.e., ε_{Th}, the search efforts in MIDACO are greatly reduced. Therefore, the prosed optimization method is tuned accordingly using the parameters FOCUS and FSTOP. The former parameter can guide the search efforts of MIDACO towards a local region, which is known to have the desired threshold, whereas the latter parameter will terminate the algorithm once the objective function exceeds that threshold [33]. Subsequently, as in Equation (37), the GBFS objective function to obtain ζ_1 and ζ_2 is provided as:

$$\mathscr{F}(x_0) = w_1 \cdot max\{|\Delta V'_{in}|\} + w_2 \cdot |\Delta V_1|, \tag{37}$$

$$x_0 = \{\zeta_1, \zeta_2\}, \tag{38}$$

$$0 < \zeta_1 \le 3, \tag{39}$$

$$0 < \zeta_2 \le 3, \tag{40}$$

where w_1 and w_2 are weights of $|\Delta V'_{in}|$ and $|\Delta V_1|$ and equal to 1 for enhanced convergence [52]. x_0 is the decision variable for the objective function $\mathscr{F}(x_0)$ in the GBFS implementation.

3.2. Objective Function for Dump Load Stochastic Optimization

In this study, four objective functions are defined as the expected total microgrid cost (TMC), the expected maximum voltage error (MVE), the expected frequency deviation ($|\Delta f|$), and the expected total energy loss (TEL). Those objectives are constructed considering all reduced scenarios NR spanning across the chosen off-peak horizon (i.e., 12–7 am). Consequently, an objective function $\mathscr{F}_i(x_1)$ with the decision variable x_1 is defined as:

$$\mathscr{F}_i(x_1) = \{\text{TMC}, \text{MVE}, |\Delta f|, \text{TEL}\}, \tag{41}$$

$$x_1 = \{P_{DL}, Q_{DL}, mn_{DL}, N_{DL}\}, \tag{42}$$

where P_{DL}, Q_{DL}, are, respectively, the dump load's active and reactive powers. N_{DL} is the DL bus location. mn_{DL} refers to the optimal droop setting considering the allocation of DL. The value of mn_{DL} influences DG droops as follows:

$$m_{pi} = mn_{DL}, \tag{43}$$

$$n_{qi} = 10 \cdot mn_{DL}, \tag{44}$$

Having reactive droop slightly above the active droop value is common and known to further improve the load-flow convergence [19,55]. Moreover, an aggregated sum for

all *NR* deterministic problems within each hour that belong to the set ($\mathscr{H}$) defining the off-peak horizon is given as total expected objective function $\breve{\mathscr{F}}_\iota(x_1)$:

$$\breve{\mathscr{F}}_\iota(x_1) = \begin{cases} \breve{\mathscr{F}}_1(x_1) = \sum\limits_{h=1}^{H} \sum\limits_{s=1}^{NR} \mathscr{F}_1^{h,s}(x_1) \cdot \Lambda_s^N \\ \breve{\mathscr{F}}_2(x_1) = \max\limits_{h \in \mathscr{H}} \left\{ \sum\limits_{s=1}^{NR} \mathscr{F}_2^{h,s}(x_1) \cdot \Lambda_s^N \right\} \\ \breve{\mathscr{F}}_3(x_1) = \max\limits_{h \in \mathscr{H}} \left\{ \sum\limits_{s=1}^{NR} \mathscr{F}_3^{h,s}(x_1) \cdot \Lambda_s^N \right\} \\ \breve{\mathscr{F}}_4(x_1) = \sum\limits_{h=1}^{H} \sum\limits_{s=1}^{NR} \mathscr{F}_4^{h,s}(x_1) \cdot \Lambda_s^N \end{cases} \tag{45}$$

where H is the total number of hours with a set $\mathscr{H}$. An expected non-dominated solution using the Pareto front optimization technique, MIDACO, is used to find x_1 that satisfies all constraints and minimizes Equation (45). The stochastic objective function $\breve{\mathscr{F}}_\iota(x_1)$ is solved by aggregating all deterministic optimization problems' objective function ($\mathscr{F}_\iota^{h,s}(x_1)$) in a solution matrix (SM) of size $H \times NR$. The four objectives are detailed as follows:

3.2.1. Total Microgrid Cost

The four base cost functions making up the TMC objective described in this work which are also dispersed throughout the off-peak horizon for each reduced scenario are given as fuel cost (FC), maintenance cost (MC), emissions cost (EC), and technical costs (TC). Such a combination is the preferred idea when considering the typical technical, environmental, and economic goals for any IMG optimization task. Furthermore, we implicitly reduce emissions and losses by including active power generation from all dispatchable DGs as a component in the TMC objective. Therefore, it would be unnecessary to include a separate objective to address emissions due to the linear relation between active power and emissions. Nevertheless, network losses should be tackled as a separate objective since the relationship between apparent power and branch current components is not linear. Conversely, the TMC cost function considered herein is based on MG operational and running costs. Thus, it does not include capital or standing costs of the MG such as DL or storage installation costs. It is a common practice in the literature to neglect other form of costs apart from running costs, as they are mainly dependent on dispatchable unit generation [24,56–58]. Moreover, as per the notion of this study, DL application should at least offset the costs of storage installation for the same purpose. Nonetheless, a complete cost benefit analysis of DL and battery EMS is given separately in the discussion section. Given the foregoing, TMC is obtained as [56,57]:

$$\mathscr{F}_1^{h,s}(x_1) = TMC_h^s = FC_h^s + MC_h^s + EC_h^s + TC_h^s, \tag{46}$$

$$FC_h^s = (\psi_{fuel}/\eta_P) \cdot \sum\nolimits_{i \in \mathscr{G}\mathscr{K}} P_{Gi}^{h,s}, \tag{47}$$

$$MC_h^s = \psi_{main} \cdot \sum\nolimits_{i \in \mathscr{G}\mathscr{K}} P_{Gi}^{h,s}, \tag{48}$$

$$EC_h^s = \Psi_{emis} \cdot \psi_{emis} \cdot \sum\nolimits_{i \in \mathscr{G}\mathscr{K}} P_{Gi}^{h,s}, \tag{49}$$

$$TC_h^s = RC_h^s + FRC_h^s, \tag{50}$$

where for a scenario s during the off-peak hour h, the total microgrid, fuel, maintenance, emissions, and technical costs are given by TMC_h^s, FC_h^s, MC_h^s, EC_h^s, TC_h^s, respectively. The dispatchable DG's generated active power is given by $P_{Gi}^{h,s}$. In addition, the reactive and frequency costs are given by RC_h^s and FRC_h^s, respectively. η_P is the efficiency in fuel consumption by a dispatchable DG. Ψ_{emis} is the dispatchable DG's emissions rate. ψ_{fuel},

ψ_{main}, and ψ_{emis} are, respectively, the fuel, maintenance, and emissions cost coefficients, noting that the technical cost is about MG reliability and stability as represented by RC_h^s and FRC_h^s costs. Reactive power is not connected with fuel, albeit leading to increased losses and penalties for generating reactive power [57]. Conversely, when frequency deviations are out of the permissible range, the FRC_h^s costs are required to ensure MG supply quality. Although technical costs often refer to $V-f$ deviations concurrently, in this article, only frequency penalty costs were elected. This is due to the fundamental role of frequency in IMG supply quality and the stringent permissible tolerance for frequency in the system ($\pm 0.4\%$) [59]. Accordingly, RC_h^s and FRC_h^s are provided by [56,57]:

$$RC_h^s = \Psi_{var} \cdot (FC_h^s + MC_h^s + EC_h^s) \cdot \frac{\sum_{i \in \mathscr{G}\mathscr{K}} Q_{Gi}^{h,s}}{\sum_{i \in \mathscr{G}\mathscr{K}} P_{Gi}^{h,s}}, \tag{51}$$

$$FRC_h^s = \psi_{freq} \cdot \left(f_{ss}^{h,s} - f_0\right), \tag{52}$$

where Ψ_{var} is the dispatchable DG's reactive power coefficient [60]. $f_{ss}^{h,s}$ is the IMG steady state frequency at scenario s during the off-peak hour h. ψ_{freq} is a penalty cost coefficient for frequency [56,59]. $Q_{Gi}^{h,s}$ is the reactive generated power by the dispatchable DG at scenario s during the off-peak hour h. Additionally, DCIMG quality of supply as well as safe operating constraints necessitate the provision of technical costs [56]. It is known that a renewable DG does not cause emissions since it consumes zero fuel. Furthermore, each WT in this article was assumed in maximum power point tracking (MPPT) control, acting as an induction generator with a 0.9 leading power factor [24,61].

3.2.2. Maximum Voltage Error

In an IMG, a good stability and reliability indicator is the voltage. Therefore, many DG allocation studies have opted for stability indices such as total voltage variations and voltage stability index. Nonetheless, the allocation herein is for DL and not DGs. Thus, a flattened voltage profile is desired to ensure system voltages as close to nominal as possible. As a result, MVE was elected to attain voltage error minimization across the IMG, and is provided by [38]:

$$\mathscr{F}_2^{h,s}(x_1) = MVE_h^s = \max_{i \in \mathscr{N}} \left\{ \left| |V_{in}^{h,s}| - 1 \right| \right\} \tag{53}$$

where $V_{in}^{h,s}$ is bus i voltage at scenario s during the off-peak hour h.

3.2.3. Frequency Deviation

On the other hand, the expected IMG frequency error is achieved as follows:

$$\mathscr{F}_3^{h,s}(x_1) = |\Delta f_h^s| = \left| m_{pT} \cdot \left(P_{G1}^{h,s} - \mathscr{R}\left\{ V_1^{h,s} \cdot B_1^{h,s^*} \right\} \right) \right| \tag{54}$$

where $V_1^{h,s}$, $B_1^{h,s}$, and $P_{G1}^{h,s}$ are, respectively, the voltage, branch current, and the active power at the VB within a scenario s during the off-peak hour h.

3.2.4. Total Energy Loss

As for the fourth objective, the expected total energy loss, it is calculated as follows:

$$\mathscr{F}_4^{h,s}(x_1) = P_{loss}^{h,s} \cdot t^s = \sum_{i=1}^{n-1} \mathscr{R}\{Z_i\} \cdot \left| B_i^{h,s} \right|^2 \cdot t^s \tag{55}$$

where, for each scenario s during the off-peak hour h, the active power loss and the branch current are given by $P_{loss}^{h,s}$ and $B_i^{h,s}$, respectively. t^h is the time duration at each s scenario which is equal to one hour.

3.3. Constraints for Dump Load Stochastic Optimization

In any IMG, there are different technical constraints that must be satisfied to ensure adequate and stable operation [3,62]. Moreover, for each deterministic optimization problem, load flow must converge for any given scenario s and off-peak hour h. This very stable behavior signals power balance constraint adherence. Moreover, for each objective function evaluation the frequency, thermal, bus voltage, and dispatchable DG power limits must be adhered concurrently. These constraint functions ($g_i^{h,s}(x_1)$) are handled during each scenario s at any given off-peak hour h as follows.

Bus i's voltage limits:

$$0.95 \leq \left| V_{in}^{h,s} \right| \leq 1.05, \tag{56}$$

Thermal limits:

$$\left| B_i^{h,s} \right| \leq \left| B_{i\_max} \right|, \tag{57}$$

Steady-state frequency limits:

$$0.996 \leq f_{ss}^{h,s} \leq 1.004, \tag{58}$$

Dispatchable DG power output limits:

$$0 \leq P_{Gi}^{h,s} \leq 4, \tag{59}$$

$$0 \leq Q_{Gi}^{h,s} \leq 2.5, \tag{60}$$

According to the presumption herein, non-dispatchable units operate with an MPPT algorithm (i.e., in PQ mode). Therefore, in any given scenario, the WT will always remain within power limits and thus were excluded from the constraint-handling function. Inversely, the limits for the decision variable x must be satisfied once at every function evaluation after the aggregated effect of all NR scenarios during low load hours (i.e., $\forall h \in \mathcal{H}$) are taken into consideration. Thus, neither DL location, DL size, nor DG droop gains are affected by scenario or hour change. These are provided as follows [28]:

DL size limits:

$$0.002 \leq P_{DL} \leq 1, \tag{61}$$

$$0.002 \leq Q_{DL} \leq 1, \tag{62}$$

Droop coefficient limits:

$$10^{-4} \leq mn_{DL} \leq 0.05 \tag{63}$$

Noteworthy is that the per-unit system was used to write all numerical data using system nominal frequency as 50 Hz, power base 500 kVA, and 12.66 kV and 11 kV as voltage base for the 69-bus and 118-bus systems, respectively.

4. Results and Discussion

The case studies considered for the IMG in this work are the IEEE 69-bus and 118-bus systems which are shown in Figure 5a,b, respectively.

System line and load data were obtained from [63,64] for the 69-bus and 118-bus systems, respectively, while the 69-bus and 118-bus system generation bus locations were obtained from [26,65], respectively. All DGs and MG ratings are given in Table 1 for the dispatchable and non-dispatchable units which were obtained from [24,58], respectively. Furthermore, it was assumed that all non-dispatchable DGs were WT units, while dispatchable DGs, on the other hand, were installed as natural gas turbine (NGT) units. The DG arrangements for the no DL case (i.e., the base case) are given, respectively, in Tables 2 and 3 for the IEEE 69-bus and 118-bus systems. The pre-islanding reference generation for all NGT units were assumed as 2.545 + j1.909 p.u. at 0.8 lagging power factor, while WT

units, on the other hand, were rated at 0.5 MW capacity with 0.9 leading power factor operation [24]. Due to the expected large power mismatch as per the notion of this study, two and four identical DLs were considered in the stochastic optimization problem for the 69-bus and 118-bus systems, respectively. The DLs were rated at 500 kVA each and allocated simultaneously with the same size and to the same location for both test systems.
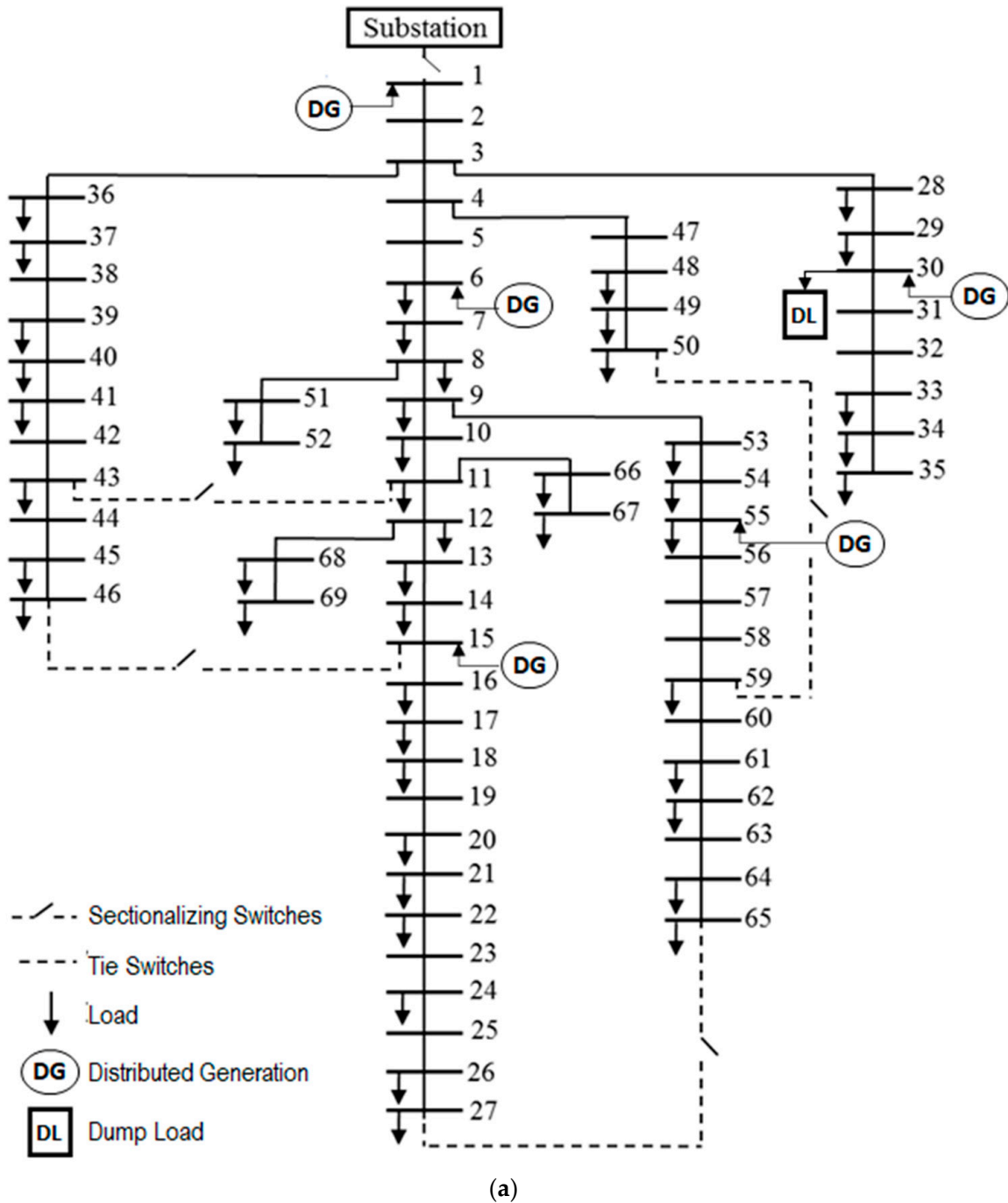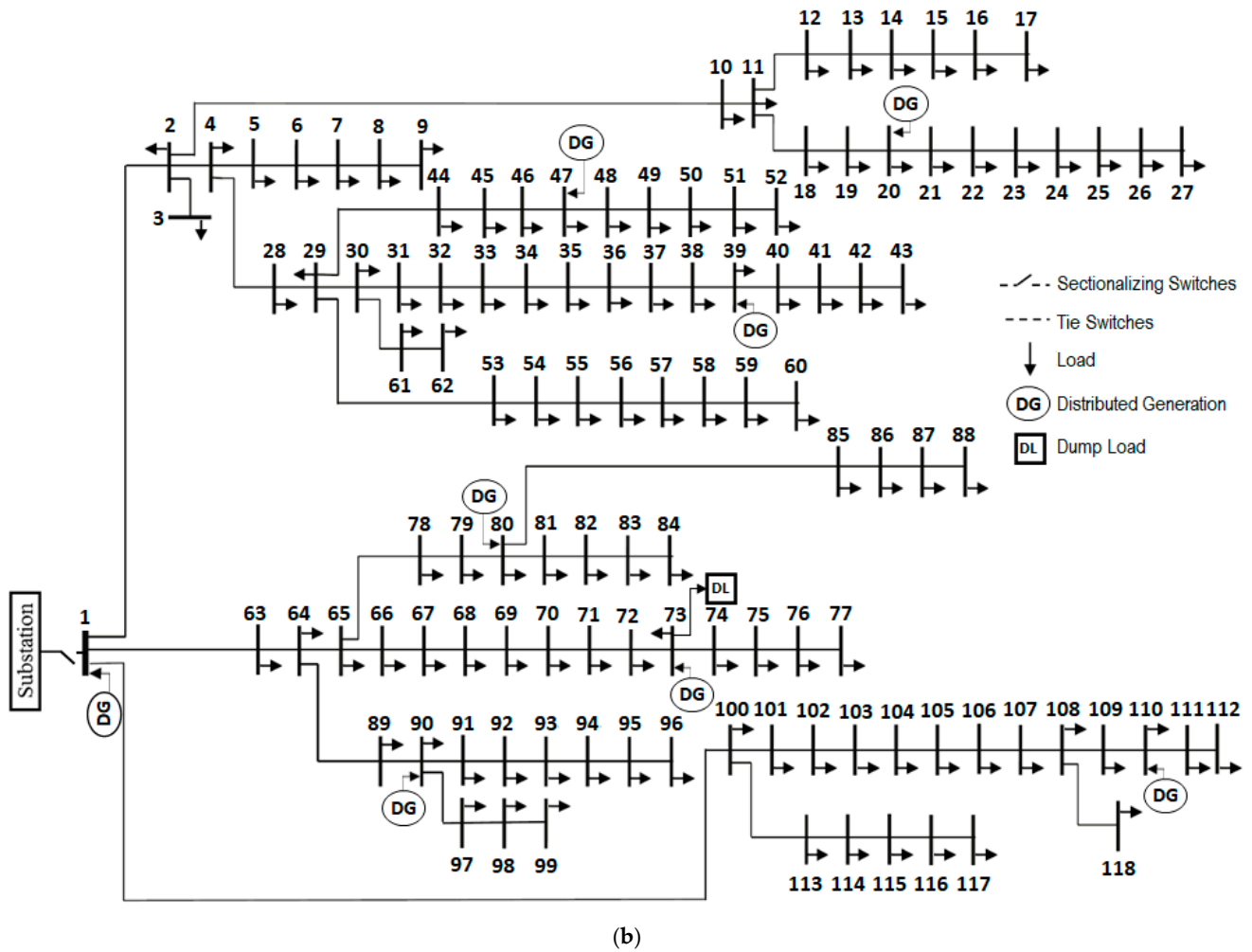

(a)

Figure 5. *Cont.*

(b)

Figure 5. The microgrid single-line diagram as modified for islanding operation for: (**a**) IEEE 69-bus (**b**) IEEE 118-bus.

Table 1. Technical characteristics of DG units and MGs under study.

NGT		WT		Others	
Parameter	**Value**	**Parameter**	**Value**	**Parameter**	**Value**
P_{min} (MW)	0.20	v_r (m/s)	10.5	Ψ_{var}	0.3
P_{Nr} (MW)	2.00	P_{Wr} (MW)	0.5	ψ_{freq} ($/Hz)	100
η_P	0.37	v_{ci} (m/s)	4.5	-	-
Ψ_{emis} (Tonne/MWh)	0.2016	v_{co} (m/s)	22.0	-	-
ψ_{emis} (USD/Tonne)	40.7	v_μ (m/s)	10.5473	-	-
ψ_{fuel} (USD/MWh)	20.5	v_σ (m/s)	3.7282	-	-
ψ_{main} (USD/MWh)	3.0	-	-	-	-

Table 2. DG unit arrangements for 69-bus system.

DG Unit	DG Type	No. of Units	Bus No.	m_{pi}	n_{qi}
DG_1	NGT	1	1	−0.05	−0.05
DG_2	NGT	1	6	−1	−1
DG_3	NGT	1	15	−0.1	−0.1
DG_4	WT	1	30	-	-
DG_5	WT	1	55	-	-

Table 3. DG unit arrangements for 118-bus system.

DG Unit	DG Type	No. of Units	Bus No.	m_{pi}	n_{qi}
DG_1	NGT	2	1	−0.05	−0.05
DG_2	NGT	2	20	−1	−1
DG_3	NGT	2	39	−0.1	−0.1
DG_4	NGT	2	47	−1	−1
DG_5	NGT	2	73	−0.2	−0.2
DG_6	WT	2	80	-	-
DG_7	WT	2	90	-	-
DG_8	WT	2	110	-	-

The simulation was modeled and executed in MATLAB®® environment on hardware comprising an Intel core i7 2.6 GHz 8 GB RAM. Furthermore, the stochastic optimization problem was initialized for each deterministic problem with 0, 0, and 10^9 values for ANTS, KERNEL, and ORACLE, respectively. Meanwhile, PARETOMAX, BALANCE, and EPSILON were set to 1000, 0, and 0.01, respectively. The parameter selection is recommended at the respective values to allow for the best mix between exploration, exploitation, and speed [33]. Lastly, to initialize the GBFS optimization problem [52,66], the parameters FSTOP and FOCUS were set to 10^{-8} and 100, respectively. A hard-stopping criterion is chosen for MIDACO by fixing the maximum number for function evaluations, known as MAXEVAL, to 10,000.

4.1. Multi-Objective Optimization

As discussed previously, by concurrently considering all 20 reduced scenarios as per the desired accuracy rate, the formulated many-objective stochastic problem was created to minimize the expected TMC, MVE, $|\Delta f|$, and TEL. Moreover, the chosen sampling rate for uncertainty modeling has resulted in NR deterministic optimization problems, each with constant load and wind power. It should be noted that the locations of DGs within each test IMG were selected to minimize losses while meeting network demand without relying on any external sources [65]. Based on the forgoing, a non-dominated solution that considers all scenarios during the off-peak horizon for each expected objective function in the stochastic optimization problem is given in Table 4.

Table 4. Multi-objective expected results considering stochastic scenarios.

Test System	69		118	
Allocation Case	No DL	With DL	No DL	With DL
N_{DL}	-	30	-	73
P_{DL}**(p.u.)**	-	1.2831	-	1.7670
Q_{DL}**(p.u.)**	-	0.4004	-	0.2389
mn_{DL}	-	0.0014	-	0.0003
TMC (USD)	6991.7	831.30	7635.6	941.61
MVE(p.u.)	0.0937	0.0245	0.1024	0.0324
$\|\Delta f\|$**(p.u.)**	0.1901	0.0022	0.2405	0.0005
TEL(kWh)	200	228.9	1472.8	1270.3
Time (s)	-	638	-	872

First step size only for $|\Delta f|$.

Similarly, the utopia–nadir balance approach has resulted in finding the optimal non-dominated solution at the center of the Pareto front to satisfy all objectives. The non-dominated solution is highlighted in green as depicted in the Pareto front for the IEEE 69-bus and 118-bus systems in Figure 6a,b, respectively. According to results, the

consideration of uncertainty in load forecast and wind speed in the DL allocation problem has resulted in costs savings, better voltage profile, and optimal supply quality if compared to the base case (i.e., without DL allocation while using droop sets of Table 2 or Table 3). Taking the TMC for the base case in particular, a significant increase in MG costs is observed against the DL allocation cases of both test systems. This is attributed to the higher fuel consumption and emissions by the dispatchable DGs in the IMG without DL. Furthermore, higher technical costs were incurred for operating the IMG without DL allocation, that is, to guarantee supply quality. Conversely, a smoother frequency profile is observed for both test systems utilizing the DL as a power management solution according to the improved expected $|\Delta f|$ during the off-peak hours as provided in Table 4.
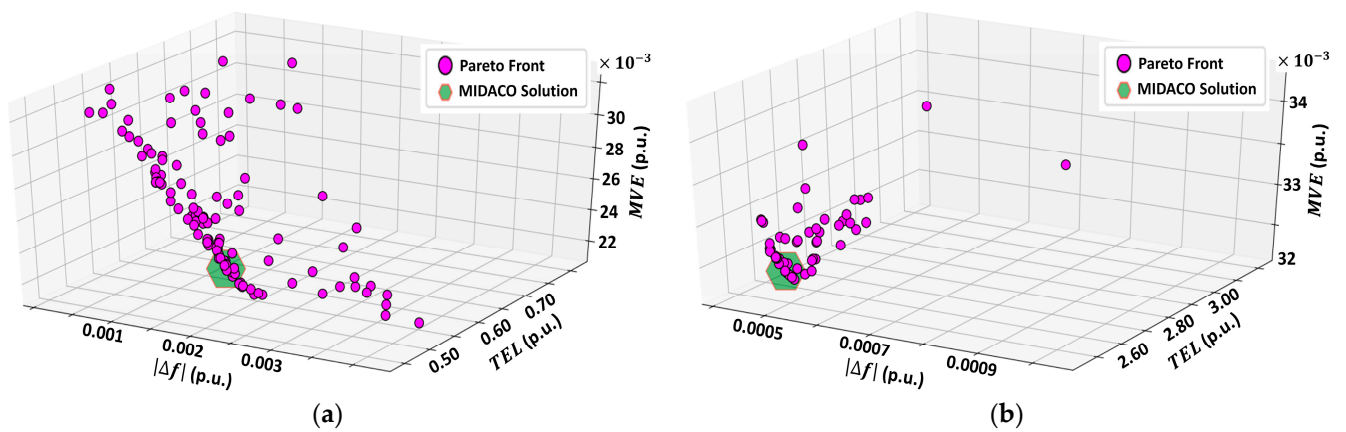

Figure 6. Pareto front of the many-objectives stochastic problem. The optimal solution as derived with the utopia–nadir balance approach is highlighted by the green hexagon shape for (**a**) 69-bus; (**b**) 118-bus.

Moreover, flatter voltage profiles were achieved by DL's optimal sizing as well as DG's optimal droop setting as depicted in Figures 7 and 8 for the 69-bus and 118-bus systems, respectively. Meanwhile, the advantage of DL allocation in DCIMG has significantly reduced the expected averaged over-frequency by 0.1847 p.u. and 0.2114 p.u. for the 69-bus and 118-bus systems, respectively, against the base case. The advancements in frequency profiles are provided in Figures 9 and 10 for the 69-bus and 118-bus systems, respectively.
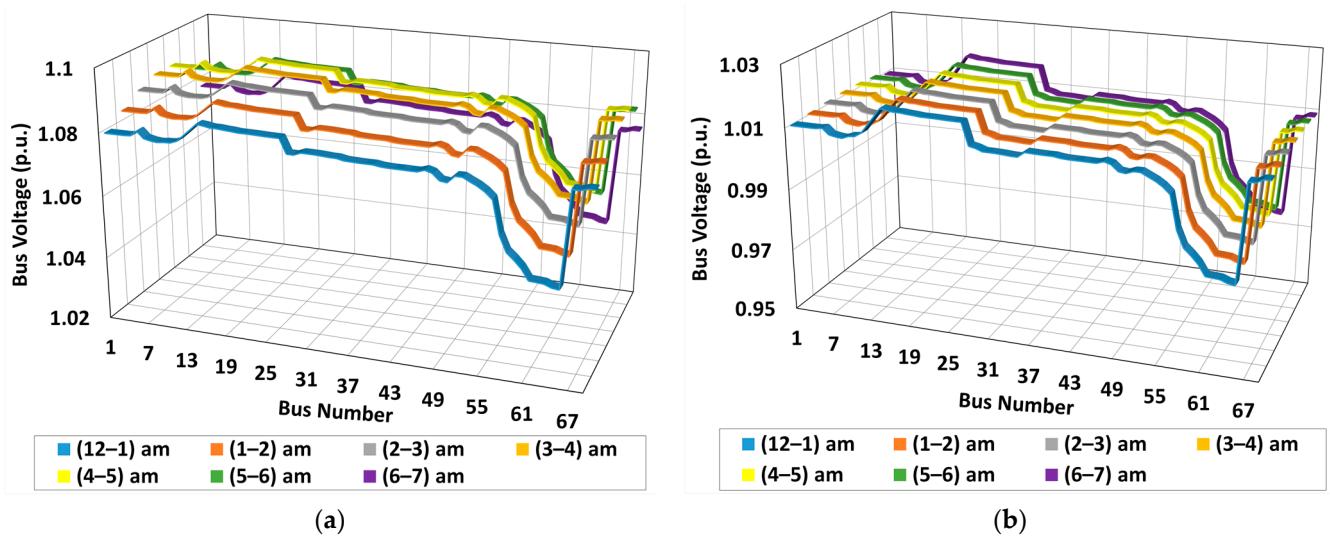

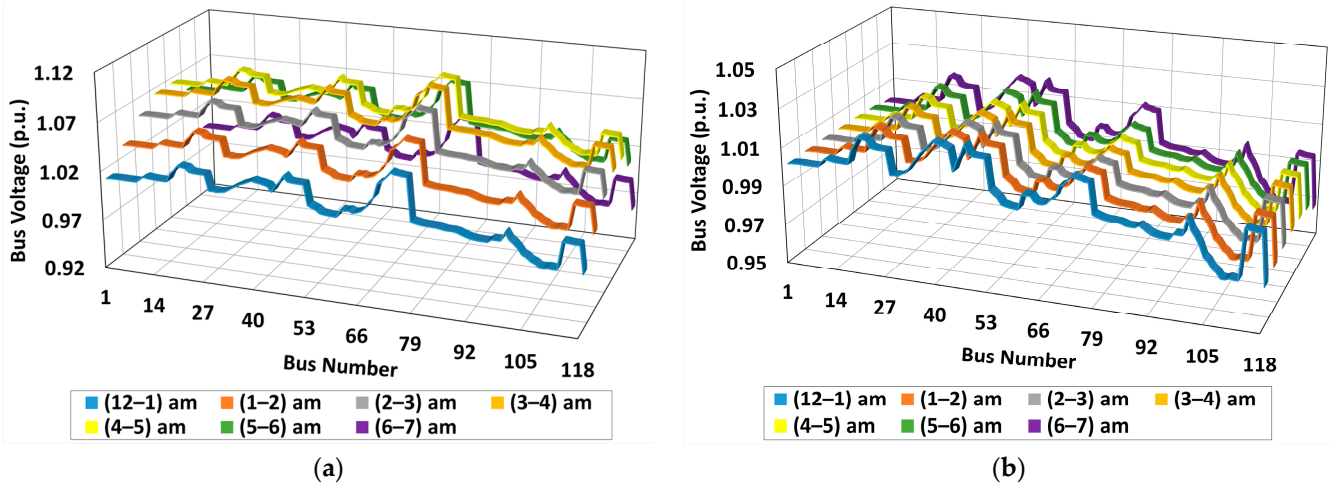**Figure 7.** Expected off-peak-hours voltage profiles for 69-bus system: (**a**) No DL; (**b**) With DL.

Figure 8. Expected off-peak-hours voltage profiles for 118-bus system: (**a**) No DL; (**b**) With DL.
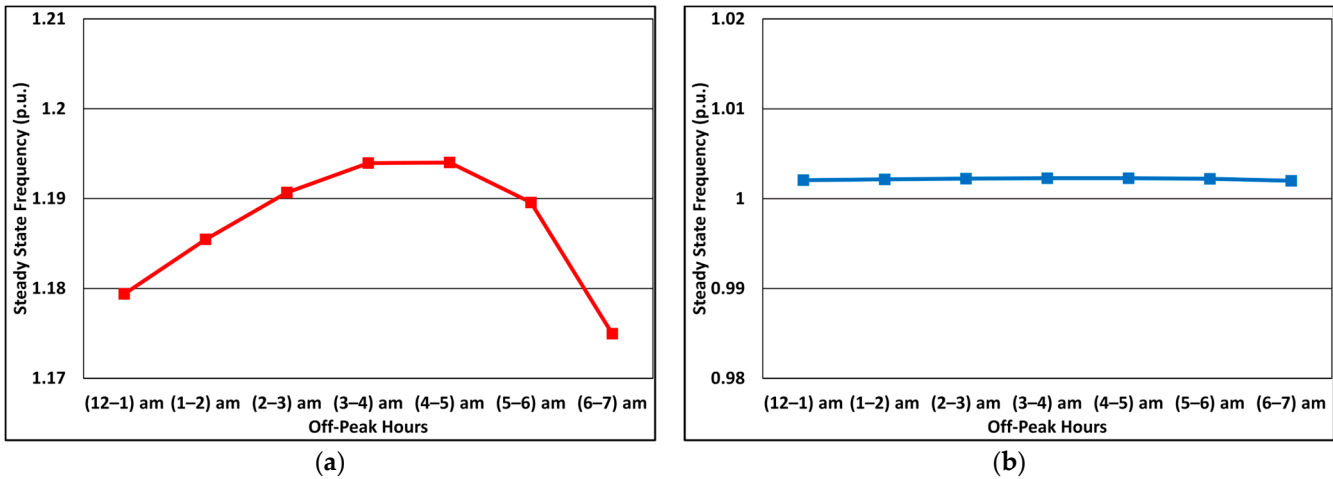

Figure 9. Expected off-peak-hours frequency profile for 69-bus system: (**a**) No DL; (**b**) With DL.
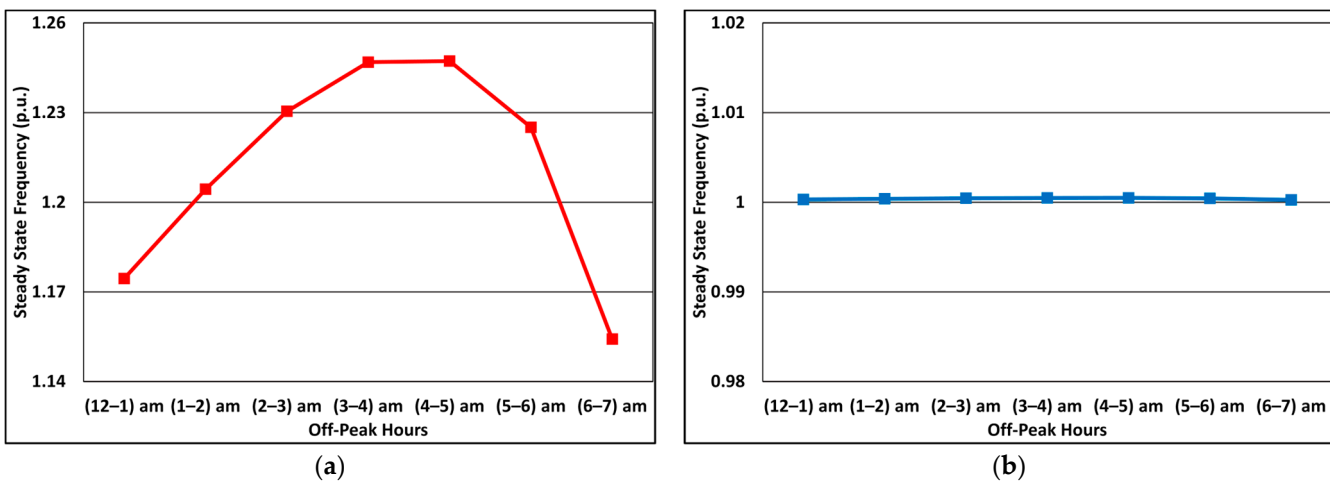
Figure 10. Expected off-peak-hours frequency profile for 118-bus system: (**a**) No DL; (**b**) With DL.

As for the fourth objective (i.e., TEL), it is generally affected by the pre-existing reactive power mismatch in the IMG. In one hand, for an IMG with relatively small reactive power mismatch, the resultant TEL will be greater after the DL inclusion. On the other hand, when the pre-existing reactive power mismatch is relatively large, the resultant TEL will be lower

after DL inclusion into the MG. This situation is explained after examining the reactive power compensation in predominantly capacitive networks and the role of DL allocation in IMGs. Notwithstanding the size of the existing reactive power mismatch before DL allocation into the network, considering TEL criterion within the many-objectives DL allocation will ensure loss reduction. Those refer to losses that would have been otherwise incurred by the general DL utilization in distribution networks as seen from the single- and two-objectives results for the DL allocation presented in [28].

4.2. Comparison with Other Metaheuristics

The efficacy of the expected non-dominated solution offered by the proposed method herein is compared against other acclaimed evolutionary and swarm intelligence techniques, viz., multi-objective genetic algorithm (MOGA) [67], multi-objective particle swarm optimization (MOPSO) [68,69], and the non-dominated sorting genetic algorithm (NSGA-II) [70,71]. The parameters for MOPSO, NSGA-II, and MOGA, were adopted from [28]. Accordingly, 11 parameters were initialized for MOPSO, namely, population and repository size both 100, leader and deletion selection pressures both 2, and starting and ending inertia weights values 0.5 and 0.001, respectively. The cognitive and social learning coefficients were 0.1 and 0.2, respectively, grid per dimension 7, and mutation rate 0.1. As for NSGA-II, four parameters were set: population size 100, distribution index for mutation 20, distribution index for crossover 100, and mutation probability 0.25. Lastly, MOGA's population size was 100, crossover probability 0.8, and mutation probability 0.001. The results obtained by each metaheuristic technique are given in Table 5.

Table 5. Comparison of expected results against different methods.

Method	MOGA		NSGA-II		MOPSO		MIDACO	
Bus System	69	118	69	118	69	118	69	118
N_{DL}	30	79	28	62	49	69	30	73
P_{DL}(p.u.)	1.5624	2.0357	1.2834	1.7750	1.6615	2.3868	1.2831	1.7670
Q_{DL}(p.u.)	0.9545	0.4547	0.6879	0.4463	0.6033	1.1205	0.4004	0.2389
mn_{DL} (p.u.)	0.0014	0.0003	0.0015	0.0003	0.0014	0.0003	0.0014	0.0003
TMC(USD)	896.36	957.71	834.00	944.68	916.69	972.57	831.30	941.61
MVE(p.u.)	0.0262	0.0387	0.0254	0.0419	0.0250	0.0330	0.0245	0.0324
$\|\Delta f\|$**(p.u.)**	0.0021	0.0005	0.0022	0.0005	0.0020	0.0004	0.0022	0.0005
TEL(p.u.)	0.4951	3.1302	0.4616	2.9582	0.5296	3.0059	0.4578	2.5405
MAXEVAL	400	400	200	200	400	400	10,000	10,000
Time [a] (s)	9763	12,061	12,203	12,843	7617	9214	638	872

[a] Algorithm computation time, first step size only for $|\Delta f|$.

According to results, an overall best for TMC and TEL was found by MIDACO for the 69-bus system, whereas MIDACO's TEL for the 118-bus system was substantially smaller if considered against the other methods. Inversely, taking the $|\Delta f|$ obtained by all methods as reference, the superiority of the proposed method is exemplified by the quality of the non-dominated solution achieved. Moreover, both MIDACO and NSGA-II have returned close values for TMC; nonetheless, the attained objectives of *TEL* and MVE were worst from NSGA-II compared to MIDACO's. Despite having much lower maximum function evaluation parameter, i.e., MAXEVAL, by MOPSO, MOGA, and NSGA-II, their recorded calculation times, albeit utilizing a parallelization strategy, were quite long, rendering them not practical. Noteworthy is that the DL locations attained by the four metaheuristics are not similar. This is attributed to the challenging and complex nature of many-objective optimization problems. Nonetheless, the handling of integer domains within MIDACO is enhanced to avoid premature convergence of the internal ACOmi instances [31]. On the other hand, the competitive edge offered by MIDACO's fine-grained parallelization

strategy was demonstrated by having much lower calculation times despite the huge number of function evaluations. The speed and accuracy advantage of MIDACO against the other metaheuristics proposed herein, shall indeed facilitate a competitive solution with decent and practical speeds. This is necessary for real-time optimization of challenging and stochastic MINLPs forming future IMGs.

4.3. Cost Benefit Analysis

As discussed in the optimization problem formulation, DL allocation is expected to reduce total running costs of the MG; that is, by considering fuel, maintenance, emissions, and technical cost reduction because of optimal dispatchable units' generation. Nonetheless, the assumption was that DL costs are offset by utilization of the power into useful operations rather than having it stored or dissipated. Therefore, to demonstrate the effectiveness of the proposed DL-based EMS (DLEMS), a cost benefit analysis (CBA) was conducted. The attained results of this analysis will signify the DL solution's advantage against a battery-based EMS (BEMS). By considering CBA for DLEMS and BEMS, the costs associated with DL and BESS installations will be analyzed, respectively. Thus, to put the CBA into practical perspective, the advantage of using DLEMS against BEMS considering power regulation in primary off-peak hours is investigated. This implies that the CBA has considered two unique EMS approaches to provide a system's hot water demand, namely, DLEMS and BEMS. In the former EMS approach, the overgeneration of excess power is absorbed by DL, while a portion of the system's demand for water-heating boilers and pumps is covered by the DL active and reactive powers, respectively [27]. Furthermore, the remainder of hot water demand is supplied by electric-powered boilers from non-renewable sources. Conversely, for BEMS implementation, BESS is utilized to store the excess overgeneration power mismatch, while the system demand for hot water is supplied by natural-gas-fired boilers and pumps.

The motivation for the CBA herein is to provide a comprehensive economic dimension as a reflection from the DL solution to the $V-f$ regulation in highly penetrated IMG. Therefore, a more realistic approach was adopted in this study contrary to that provided in [27]. This was performed by considering all capital, fuel, maintenance, and running costs for hot water system installation and maintenance. Moreover, by considering uncertainties in wind and load powers, the amount of available power to be dumped was determined using stochastic scenario-based modeling. Additionally, in addition to assuming the levelized cost of energy (LCOE) for storage solutions in [27], the CBA herein has considered LCOE for gas and electric water-heating systems. Accordingly, when it comes to investment analysis for costs of producing energy, LCOE is widely used in the industry and academia to provide sufficient investment return overview for different energy technologies [72]. Subsequently, the CBA is used to measure the cost-effectiveness of relieving high power congestion during off-peak hours with a DL solution rather than a storage solution. As a result, the analysis was conducted assuming two LCOEs for electric boilers, viz., from renewable and non-renewable sourced electricity. Furthermore, the provision for the total demand for hot water is scheduled during low-load hours by storing the hot water in dedicated cylinders to be used later via on-demand water circulation systems [27,73]. The hot water volume for total daily demand (V_{hw}^{tot}) in this article is assumed on average (considering winter and summer days) as 817.06 m^3 and 1293.67 m^3 for 69-bus and 118-bus systems, respectively [24,73]. Similarly, the hot water volume (V_{hw}) equation is derived from the obtainable energy to produce heat as follows [73]:

$$V_{hw} = \frac{P_{hw} \cdot \eta_{hw} \cdot h}{C_w \cdot \rho_w \cdot \Delta T},$$

(64)

where P_{hw} is the power utilized by the boiler for heating water during h hours. ρ_w is the density of water. C_w is the specific heat of water. η_{hw} is the boiler efficiency for heating water and assumed as 0.99 and 0.80 for electric (η_{hw}^{ele}) and gas (η_{hw}^{gas}) boilers, respectively.

ΔT is the difference between the set-point temperature T_{st}, assumed at 60 °C, and the inlet temperature T_{in}, assumed at 10 °C, and is given by [27,73]:

$$\Delta T = T_{st} - T_{in}, \tag{65}$$

Due to the foregoing, the utilization of electric or gas boilers for water heating will accumulate the following costs:

$$HC_{hw}^{e} = \psi_{LCOE}^{eleR} \cdot P_{DL} \cdot h + \psi_{LCOE}^{eleN} \cdot P_{hw}^{ele} \cdot h, \tag{66}$$

$$HC_{hw}^{g} = \psi_{LCOE}^{gas} \cdot P_{hw}^{gas} \cdot h + SC_{BESS}, \tag{67}$$

$$SC_{BESS} = \psi_{LCOE}^{BESS} \cdot P_{DL} \cdot h, \tag{68}$$

where HC_{hw}^{g} and HC_{hw}^{e} are the BEMS and DLEMS costs for heating water, respectively. P_{hw}^{gas} and P_{hw}^{ele} are the power needed by gas and electric boilers to cover the total system demand for hot water, respectively. Note that P_{DL} was deducted from P_{hw}^{ele} to represent renewable-based electric boiler costs. ψ_{LCOE}^{gas} is the gas boiler LCOE coefficient, which is valued at 57.13 USD/MWh (53 EUR/MWh) [72]. ψ_{LCOE}^{eleN} and ψ_{LCOE}^{eleR} are the non-renewable- and renewable-sourced boilers' LCOE, respectively, which are valued at 70.06 USD/MWh (65 EUR/MWh) for ψ_{LCOE}^{eleN} and 33.42 USD/MWh (31 EUR/MWh) for ψ_{LCOE}^{eleR} [72]. Noteworthy is that the LCOE from [72] does not account for long distance thermal losses, nor the cost associated with long-distance thermal installation and maintenance. Nonetheless, the costs incurred from long-distance thermal operation are assumed the same for both EMSs in question and was omitted form the comparison. As for a BEMS strategy, P_{DL} (i.e., the excess power) would require storage in an appropriate BESS. This will lead to extra costs which are called storage costs (SC_{BESS}). The value of SC_{BESS} is dependent on the required storage power and the LCOE for the corresponding storage technology [74]. Accordingly, two LCOE coefficients for storage technologies are considered herein to attain a better comparison against DLEMS. Thus, two BESS types are used in the BEMS implementation, viz., Nickel–Cadmium (Ni-Cd) and Lithium-ion (Li-ion). The cost coefficients for Ni-Cd (ψ_{LCOE}^{Ni}) and Li-ion (ψ_{LCOE}^{Li}) technologies are assumed as 691.06 USD/MWh (641.1 EUR/MWh) and 658.61 USD/MWh (611 EUR/MWh), respectively [74].

All technical parameters and cost coefficients used in the CBA of this study are provided in Table 6. Lastly, the average daily hot water demand V_{hw}^{tot} is used to calculate the total cost for hot water per calendar year (HC_{hw}^{tot}). This is done for both DLEMS and BEMS implementations as follows:

$$HC_{hw}^{tot} = \begin{cases} HC_{hw}^{e} \cdot 365.25 \\ HC_{hw}^{g} \cdot 365.25 \end{cases} \tag{69}$$

Table 6. Microgrid data for CBA of water heating system.

Cost Coefficients		Technical Characteristics	
Parameter	**Value**	**Parameter**	**Value**
ψ_{LCOE}^{eleR} (USD/MWh)	33.42	T_{in} (°C)	10
ψ_{LCOE}^{eleN} (USD/MWh)	70.06	T_{st} (°C)	60
ψ_{LCOE}^{gas} (USD/MWh)	57.13	C_w (J/Kg. °C)	4200
ψ_{LCOE}^{Li} (USD/MWh)	658.61	ρ_w (Kg/m³)	997
ψ_{LCOE}^{Ni} (USD/MWh)	691.06	η_{hw}^{ele}	0.99
-	-	η_{hw}^{gas}	0.80

Provided in Table 7 are the results of the CBA for the 69-bus and 118-bus systems. According to the results, the costs associated with DLEMS to cover yearly hot water

demand were much lower than they were for BEMS. This is true for both BESS technologies implemented, i.e., Li-ion and Ni-Cd. Likewise, the estimated costs for hot water demand per calendar year using the Ni-Cd-based BEMS were USD 2,535,058.14 and USD 3,746,532.52 for the 69-bus and 118-bus systems, respectively. Similarly, using the cheaper BESS option (i.e., Li-ion) in the BEMS implementation did not result in significant cost reductions, as they were USD 2,474,229.79 and USD 3,662,771.75 for the 69-bus and 118-bus systems, respectively.

Table 7. Yearly hot water demand using different EMS strategies.

EMS Method	Using DL		Using Li-ion		Using Ni-Cd	
Test system	69	118	69	118	69	118
P_{DL} **(MW)**	0.6416	0.8835	0.6416	0.8835	0.6416	0.8835
P_{hw}^{ele} **(MW)**	5.3584	8.6165	-	-	-	-
HC_{hw}^{e} **(USD/day)**	3175	5065.90	-	-	-	-
P_{hw}^{gas} **(MW)**	-	-	7.4251	11.7563	7.4251	11.7563
HC_{hw}^{g} **(USD/day)**	-	-	6774.07	10,028.1	6940.61	10,257.4
SC_{BESS} **(USD/day)**	-	-	3380.5	4655.1	3547.1	4884.4
V_{hw}^{tot} **(m³/day)**	817.06	1293.67	817.06	1293.67	817.06	1293.67
HC_{hw}^{tot} **($/year)**	1,159,667.99	1,850,319.83	2,474,229.79	3,662,771.75	2,535,058.14	3,746,532.52
Saving method	-		Using DL instead of Li-ion		Using DL instead of Ni-Cd	
Net savings (USD/year)	-	-	1,314,561.79	1,812,452.0	1,375,390.14	1,896,212.69

On the other hand, using DLEMS for the same purpose (i.e., heating systems hot water demand per calendar year) has resulted in significant and expected reductions in costs valued at USD 1,159,667.99 and USD 1,850,319.83 for the 69-bus and 118-bus systems, respectively. The major cost factors affecting this huge difference between DLEMS and BEMS are the storage and gas boiler costs. The latter is attributed to the higher power required for gas boilers to produce the same volume of hot water if compared with the more efficient electric boilers. The amount of power required by gas boilers were 7.4251 MW and 11.7563 MW for the 69-bus and 118-bus systems, respectively. Conversely, the power required by electric boilers were just at 6 MW and 9.5 MW for 69-bus and 118-bus systems, respectively. As for the former cost factor, BESS are still expensive considering different variables such as installation, end-of-life, and replacement of batteries [74]. Moreover, despite that storage costs are dropping as technology advances, the overall cost elements of BESS are still not accounted for in medium- and long-term solutions [74].

Contrariwise, the notion of this study conforms with current norms that renewable energy penetration levels in DCIMG are rising in the foreseeable future. This will lead to higher periods of excess power mismatch that BEMS are not equipped to handle economically. Therefore, investing in more BESSs is not cost-effective as demonstrated by this CBA. Inversely, taking the DLEMS implementation for the 118-bus systems as an example, significant savings are achieved against the BEMS implementation. This is translated to huge saving of USD 1,812,452.0 and USD 1,896,212.69 for not using the Li-ion and Ni-Cd storage options, respectively. Furthermore, as mentioned previously, renewable energy is expected to increase drastically, leading to further reductions in electric boilers over all costs. Contrariwise, excess renewable power at off-peak hours will lead to more curtailment of renewable energy, higher costs of storage solutions, and loss of renewable transmission links. Therefore, an investment in DLEMS as a power management solution instead of BEMS is a more cost-effective venture.

5. Conclusions

In this article, the uncertainty surrounding demand forecast and renewable generation within the DL allocation problem to regulate $V-f$ in highly penetrated DCIMG was investigated. A scenario-based stochastic modeling of uncertainty was used to model load forecast errors and wind generation. An RWM tool was used with higher accuracy to generate 10,000 scenarios by segmenting the load and wind PDFs into 15 and 30 probability levels, respectively. The optimal DL location and size as well as optimal DG droops were determined as a many-objectives problem to account for expected TMC, MVE, $|\Delta f|$, and TEL. This was achieved using a state-of-the-art metaheuristic technique, MIDACO, combined with a robust and efficient load-flow method called GBFS. The optimization problem was applied on the IEEE 69-bus and 118-bus systems for validation. Moreover, a massive parallelization framework using the fine-grained parallelization strategy of MIDACO was utilized to handle the stochastic many-objectives problem. The proposed method has shown huge advancements in uncertainty handling via reduced calculation burden for probabilistic-based methods. Results have demonstrated the advantage of DL allocation as an off-peak power management solution for large power mismatch when considering uncertainty. Moreover, the efficacy of the proposed method was compared with different evolutionary and swarm intelligence techniques. Likewise, the obtained results by the proposed method showed better accuracy and significant speed advantage in calculation times. Moreover, the results provided by the CBA have provided a competitive economic advantage for DLEMS over BEMS as an off-peak power management solution. Future work could be extended to address a different mix of renewable and non-renewable generation, multiple dump load allocations at multiple different buses, hybrid power management systems using BESS and DL to handle power variation at peak and off-peak hours, respectively, and the modeling of other uncertainty factors such as loss of generation and inverter failure.

Author Contributions: Conceptualization, M.Z.K. and A.F.Z.; methodology, M.Z.K. and A.F.Z.; investigation, M.Z.K.; writing—original draft preparation, M.Z.K.; writing—review and editing, A.F.Z.; supervision, A.F.Z. All authors have read and agreed to the published version of the manuscript.

Data Availability Statement: The data supporting the reported results are available in the manuscript.

Conflicts of Interest: The authors declare no conflict of interest.

Appendix A

Table A1. List of Acronyms.

Acronym	Definition	Acronym	Definition
ACO	Ant Colony Optimization	MIDACO	Mixed-Integer Distributed Ant Colony Optimization
ACOmi	Mixed-Integer Ant Colony Optimization	MINLP	Mixed-Integer Nonlinear Programming
BEMS	Battery-based Energy Management System	MOGA	Multi-Objective Genetic Algorithm
BESS	Battery Energy Storage System	MOPSO	Multi-Objective Particle Swarm Optimization
BFS	Backward/Forward Sweep	MPPT	Maximum Power Point Tracking
CBA	Cost Benefit Analysis	MOGA	Multi-Objective Genetic Algorithm
DCIMG	Droop Controlled Islanded Microgrid	MOPSO	Multi-Objective Particle Swarm Optimization
DG	Distributed Generation	MVE	Maximum Voltage Error
DL	Dump Load	NGT	Natural Gas Turbine
DLEMS	Dump-Load-based Energy Management System	Ni-Cd	Nickel-Cadmium
EMS	Energy Management System	NSGA-II	Non-Dominated Sorting Genetic Algorithm
ELC	Electronic Load Controller	OPM	Oracle Penalty Method
ESS	Energy Storage System	PDF	Probability Density Function
GBFS	General Backward/Forward Sweep	p.u.	Per Unit
IBDG	Inverter-Based Distributed Generation	RES	Renewable Energy Resources

Table A1. *Cont.*

Acronym	Definition	Acronym	Definition
IMG	Islanded Microgrid	RWM	Roulette Wheel Mechanism
LCOE	Levelized Cost of Energy	SBFS	Special Backward/Forward Sweep
Li-ion	Lithium-ion	TEL	Total Energy Loss
MCS	Monte Carlo Simulation	TMC	Total Microgrid Cost
MG	Microgrid	VB	Virtual Bus
MGCC	Microgrid Central Controller	WT	Wind Turbine

Table A2. List of Symbols and Nomenclatures.

Symbol	Definition	Symbol	Definition
f, f_0, f_{ss}	Operating, reference, and steady state frequency	Q_c	Average reactive power correction factor in the system
$V-f$	Voltage and Frequency	$P-f, Q-V$	Active power-Frequency, Reactive power-Voltage
V_i, V_0	Operational and reference voltage at bus i	ΔQ_{Gi}	Reactive power error vector
P_{Gi}, P_{Gi0}	Generated and reference active power at bus i	β	A Boolean constant to enable reactive power correction
Q_{Gi}, Q_{Gi0}	Generated and reference reactive power at bus i	Q'_{Gi}	Desired reactive power at bus i
$\phi_W(v)$	Wind speed probability density function	U_i, N_i	The objective function's utopia and nadir values
k_s, c_s	Weibull distribution shape factor and scale index	w_i^J	Matrix of weights for each sub-problem
v	Wind speed	$d_i^J(x), D_J(x)$	Solution x weighted and average distance
μ_W, σ_W	Average and standard deviation for wind speed	$B_J(x)$	The balance function
W_{st}	Wind speed state	$T_J(x)$	The target function
$\Lambda(W_{st})$	Probability of occurrence for a wind speed state	ζ_1, ζ_2	Dynamic damping factors for GBFS
v_{st}^u, v_{st}^l	Upper and lower limits for wind speed state	x_0	GBFS decision variable
v_{st}	Mean wind speed during wind state W_{st}	$\mathscr{F}(x_0)$	GBFS objective function
P_{Wr}	Rated wind turbine power	TMC_h^s	Total microgrid cost at scenario s during off-peak hour h
v_{co}, v_{ci}	Cut off and cut-in wind speeds for the wind turbine	$FC_h^s, MC_h^s, EC_h^s, TC_h^s$	Fuel, maintenance, emissions, and technical costs at scenario s during off-peak hour h, respectively
v_μ	Wind site average speed	RC_h^s, FRC_h^s	Reactive and frequency costs at the scenario s during the off-peak hour h, respectively
v_r	Rated wind turbine speed	$P_{Gi}^{h,s}, Q_{Gi}^{h,s}$	Active and reactive powers generated by dispatchable DG unit at the scenario s during the off-peak hour h
P_{Li}^s, Q_{Li}^s	Load's active and reactive random powers in scenario s	$\psi_{fuel}, \psi_{main}, \psi_{emis}$	Fuel, maintenance, and emissions cost coefficients, respectively
P_{Wi}^s	Wind turbine's active random power in scenario s	Ψ_{emis}	Emissions rate by the dispatchable DG
Ω_s	A set of all random variables in the stochastic problem	η_P	Fuel consumption efficiency by the dispatchable DG
Λ_s^N	Convolved normalized probability for a scenario s	Ψ_{var}	Reactive power coefficient of the dispatchable DG
$\mathscr{F}_t(x)$	The objective function of the MINLP problem	ψ_{freq}	Frequency penalty cost coefficient
$\mathscr{F}_t^s(x)$	Objective function value during scenario s	$f_{ss}^{h,s}$	Steady State frequency during scenario s at off-peak hour h
$\breve{\mathscr{F}}_t(x)$	The expected value for the objective function	$V_{in}^{h,s}$	Voltage at bus i considering scenario s during the off-peak hour h
P_{G1}, Q_{G1}	Virtual bus generated active and reactive powers	MVE_h^s	Maximum voltage error considering scenario s during the off-peak hour h
n_{qi}, m_{pi}	Voltage and frequency droop coefficients at bus i	$P_{G1}^{h,s}, V_1^{h,s}, B_1^{h,s}$	Active power, voltage, and branch current at the virtual bus considering scenario s during the off-peak hour h, respectively
n_{qT}, m_{pT}	Equivalent voltage and frequency droop coefficients	Δf_h^s	Frequency deviation considering scenario s during the off-peak hour h
mn_{DL}	Optimum droop settings for dump load allocation	t^h	Off-peak time duration at each s scenario
P_{DL}, Q_{DL}	Dump load's active and reactive powers	$P_{loss}^{h,s}, Q_{loss}^{h,s}$	Active and reactive power losses considering scenario s during the off-peak hour h, respectively
lk, wk, gk	The microgrid total number of loads, wind turbines, and generating units, respectively.	$B_i^{h,s}$	Branch current at scenario s during the off-peak hour h
NV	Number of uncertain variables in scenario s	NR	Number of reduced scenarios in the stochastic problem
$\mathscr{N}$	All system buses set	RC_h^s, FRC_h^s	Reactive and frequency costs at the scenario s during the off-peak hour h, respectively
$\mathscr{GK}$	Dispatchable DG buses of the microgrid as a subset of $\mathscr{N}$	x_1	Dump load problem decision variable
P_{loss}, Q_{loss}	Total microgrid's active and reactive power losses	$\breve{\mathscr{F}}_t(x_1)$	Dump load expected objective function
$\Delta V_1, \Delta f$	The virtual bus's voltage and frequency deviations	$\mathscr{G}_i^{h,s}(x_1)$	Dump load constraint handling function at scenario s during the off-peak hour h
ε_{Th}	Tolerance threshold value for convergence criteria	HC_{hw}^e, HC_{hw}^g	Water heating costs using dump load and battery energy management systems, respectively
c	Load-flow method iteration counter	SC_{BESS}	Battery storage costs

Table A2. *Cont.*

Symbol	Definition	Symbol	Definition
S_i, I_i	Apparent power and current inject at bus i	HC_{hw}^{tot}	Total yearly hot water costs
B_i	Branch current flowing from bus i to bus $i+1$	V_{hw}^{tot}	Total yearly volume of hot water
B_{i_max}	Maximum limit for branch current B_i	P_{hw}^{ele}, P_{hw}^{gas}	Power required for electric and gas boilers, respectively
Z_i, R_i, X_i	Impedance, resistance, and reactance seen by B_i	ψ_{LCOE}^{eleR}, ψ_{LCOE}^{eleN}	Levelized cost of energy for renewable and non-renewable sourced electric boilers
V_{in}	New voltage value for bus i after forward sweep	ψ_{LCOE}^{gas}	Levelized cost of energy for gas boilers
V_{in}'	The damped system voltage vector	ψ_{LCOE}^{Li}, ψ_{LCOE}^{Ni}	Levelized cost of energy for Li-ion and Ni-Cd batteries, respectively
f_c, f_{c+1}	Frequency at iterations c and $c+1$, respectively	T_{in}, T_{st}	Inlet and set-point temperature for water heating boiler
V_{1c}, V_{1c+1}	Voltage at iterations c and $c+1$, respectively	C_w, ρ_w	Specific heat and density for water, respectively.
γ_i	Reactive power correction vector	η_{hw}^{ele}, η_{hw}^{gas}	Efficiency of electric and gas boilers, respectively

References

1. Fontenot, H.; Dong, B. Modeling and control of building-integrated microgrids for optimal energy management—A review. *Appl. Energy* **2019**, *254*, 113689. [CrossRef]
2. Kumar, K.P.; Saravanan, B. Recent techniques to model uncertainties in power generation from renewable energy sources and loads in microgrids—A review. *Renew. Sustain. Energy Rev.* **2017**, *71*, 348–358. [CrossRef]
3. *IEEE Std 1547-2018*; IEEE Standard for Interconnection and Interoperability of Distributed Energy Resources with Associated Electric Power Systems Interfaces. IEEE Std 1547–2018 (Revision of IEEE Std 1547–2003); IEEE: Piscataway, NJ, USA, 2019; pp. 1–138. [CrossRef]
4. Guerrero, J.M.; Vasquez, J.C.; Matas, J.; de Vicuna, L.G.; Castilla, M. Hierarchical Control of Droop-Controlled AC and DC Microgrids—A General Approach Toward Standardization. *IEEE Trans. Ind. Electron.* **2011**, *58*, 158–172. [CrossRef]
5. Ssekulima, E.B.; Anwar, M.B.; Al Hinai, A.; El Moursi, M.S. Wind speed and solar irradiance forecasting techniques for enhanced renewable energy integration with the grid: A review. *IET Renew. Power Gener.* **2016**, *10*, 885–989. [CrossRef]
6. El-Bidairi, K.S.; Nguyen, H.D.; Mahmoud, T.S.; Jayasinghe, S.; Guerrero, J.M. Optimal sizing of Battery Energy Storage Systems for dynamic frequency control in an islanded microgrid: A case study of Flinders Island, Australia. *Energy* **2020**, *195*, 117059. [CrossRef]
7. Elrayyah, A.; Cingoz, F.; Sozer, Y. Smart Loads Management Using Droop-Based Control in Integrated Microgrid Systems. *IEEE J. Emerg. Sel. Top. Power Electron.* **2017**, *5*, 1142–1153. [CrossRef]
8. Singh, S.; Jagota, S.; Singh, M. Energy management and voltage stabilization in an islanded microgrid through an electric vehicle charging station. *Sustain. Cities Soc.* **2018**, *41*, 679–694. [CrossRef]
9. Haidar, A.M.; Muttaqi, K.M.; Sutanto, D. Technical challenges for electric power industries due to grid-integrated electric vehicles in low voltage distributions: A review. *Energy Convers. Manag.* **2014**, *86*, 689–700. [CrossRef]
10. Faisal, M.; Hannan, M.A.; Ker, P.J.; Hussain, A.; Mansor, M.B.; Blaabjerg, F. Review of Energy Storage System Technologies in Microgrid Applications: Issues and Challenges. *IEEE Access* **2018**, *6*, 35143–35164. [CrossRef]
11. Singh, R.R.; Kumar, B.A.; Shruthi, D.; Panda, R.; Raj, C.T. Review and experimental illustrations of electronic load controller used in standalone Micro-Hydro generating plants. *Eng. Sci. Technol. Int. J.* **2018**, *21*, 886–900. [CrossRef]
12. Gyawali, N.; Paudel, B.; Subedi, B. Improved active power sharing strategy for ELC Controlled Synchronous Generators Based Islanded Micro Grid application. In Proceedings of the 9th International Conference on SKIMA, Kathmandu, Nepal, 15–17 December 2015; pp. 1–5. [CrossRef]
13. Roodsari, B.N.; Nowicki, E.; Freere, P. A New Electronic Load Controller for the Self-excited Induction Generator to Decrease Stator Winding Stress. *Energy Procedia* **2014**, *57*, 1455–1464. [CrossRef]
14. Kalla, U.K.; Singh, B.; Murthy, S.S. Modified electronic load controller for constant frequency operation with voltage regulation of small hydro driven single-phase SEIG. In Proceedings of the IEEE IASAM, Addison, TX, USA, 18–22 October 2015; pp. 1–8. [CrossRef]
15. Nehrir, M.; Lameres, B.; Venkataramanan, G.; Gerez, V.; Alvarado, L. An approach to evaluate the general performance of stand-alone wind/photovoltaic generating systems. *IEEE Trans. Energy Convers.* **2000**, *15*, 433–439. [CrossRef]
16. Doolla, S.; Bhatti, T. Load Frequency Control of an Isolated Small-Hydro Power Plant with Reduced Dump Load. *IEEE Trans. Power Syst.* **2006**, *21*, 1912–1919. [CrossRef]
17. Roodsari, B.N.; Nowicki, E.P. Analysis and Experimental Investigation of the Improved Distributed Electronic Load Controller. *IEEE Trans. Energy Convers.* **2018**, *33*, 905–914. [CrossRef]
18. Sun, Q.; Huang, B.; Li, D.; Ma, D.; Zhang, Y. Optimal Placement of Energy Storage Devices in Microgrids via Structure Preserving Energy Function. *IEEE Trans. Ind. Inform.* **2016**, *12*, 1166–1179. [CrossRef]
19. Gupta, Y.; Doolla, S.; Chatterjee, K.; Pal, B.C. Optimal DG Allocation and Volt–Var Dispatch for a Droop-Based Microgrid. *IEEE Trans. Smart Grid* **2021**, *12*, 169–181. [CrossRef]

20. Dzamarija, M.; Keane, A. Autonomous Curtailment Control in Distributed Generation Planning. *IEEE Trans. Smart Grid* **2016**, *7*, 1337–1345. [CrossRef]
21. Chen, C.; Duan, S.; Cai, T.; Liu, B.; Hu, G. Optimal Allocation and Economic Analysis of Energy Storage System in Microgrids. *IEEE Trans. Power Electron.* **2011**, *26*, 2762–2773. [CrossRef]
22. Abdelaziz, M.M.A.; Farag, H.E.; El-Saadany, E.F. Optimum Reconfiguration of Droop-Controlled Islanded Microgrids. *IEEE Trans. Power Syst.* **2016**, *31*, 2144–2153. [CrossRef]
23. Marzband, M.; Parhizi, N.; Savaghebi, M.; Guerrero, J.M. Distributed Smart Decision-Making for a Multimicrogrid System Based on a Hierarchical Interactive Architecture. *IEEE Trans. Energy Convers.* **2016**, *31*, 637–648. [CrossRef]
24. Maulik, A.; Das, D. Optimal Operation of Droop-Controlled Islanded Microgrids. *IEEE Trans. Sustain. Energy* **2018**, *9*, 1337–1348. [CrossRef]
25. Jithendranath, J.; Das, D. Scenario-based multi-objective optimisation with loadability in islanded microgrids considering load and renewable generation uncertainties. *IET Renew. Power Gener.* **2019**, *13*, 785–800. [CrossRef]
26. Uniyal, A.; Sarangi, S. Optimal allocation of ELC in microgrid using droop controlled load flow. *IET Gener. Transm. Distrib.* **2019**, *13*, 4566–4578. [CrossRef]
27. Uniyal, A.; Sarangi, S.; Rawat, M.S. Optimal Dump Load Allocations in High RBDG Penetrated Microgrid for Voltage and Frequency Regulation. *Arab. J. Sci. Eng.* **2021**, *46*, 1511–1528. [CrossRef]
28. Kreishan, M.Z.; Zobaa, A.F. Allocation of Dump Load in Islanded Microgrid Using the Mixed-Integer Distributed Ant Colony Optimization. *IEEE Syst. J.* **2022**, *16*, 2568–2579. [CrossRef]
29. Schlüter, M.; Egea, J.A.; Antelo, L.T.; Alonso, A.A.; Banga, J.R. An Extended Ant Colony Optimization Algorithm for Integrated Process and Control System Design. *Ind. Eng. Chem. Res.* **2009**, *48*, 6723–6738. [CrossRef]
30. Wozniak, M.; Sikora, A.; Zielonka, A.; Kaur, K.; Hossain, M.S.; Shorfuzzaman, M. Heuristic Optimization of Multipulse Rectifier for Reduced Energy Consumption. *IEEE Trans. Ind. Inform.* **2022**, *18*, 5515–5526. [CrossRef]
31. Schlüter, M.; Egea, J.A.; Banga, J.R. Extended ant colony optimization for non-convex mixed integer nonlinear programming. *Comput. Oper. Res.* **2009**, *36*, 2217–2229. [CrossRef]
32. Schlüter, M.; Gerdts, M. The oracle penalty method. *J. Glob. Optim.* **2010**, *47*, 293–325. [CrossRef]
33. Schlueter, M.; Munetomo, M. MIDACO Solver User Manual 6.0, Hokkaido University, Sapporo, Japan, Technical Report. 2018. Available online: http://www.midaco-solver.com/data/other/MIDACO_User_Manual.pdf (accessed on 21 June 2022).
34. Schlueter, M.; Munetomo, M. Parallelization strategies for evolutionary algorithms for MINLP. In Proceedings of the IEEE CEC, Cancun, Mexico, 20–23 June 2013; pp. 635–641. [CrossRef]
35. Schlüter, M.; Gerdts, M.; Rückmann, J.-J. A numerical study of MIDACO on 100 MINLP benchmarks. *Optimization* **2012**, *61*, 873–900. [CrossRef]
36. Schlueter, M. MIDACO software performance on interplanetary trajectory benchmarks. *Adv. Space Res.* **2014**, *54*, 744–754. [CrossRef]
37. Price, W.W.; Chiang, H.D.; Clark, H.K.; Concordia, C.; Lee, D.C.; Hsu, J.C.; Ihara, S.; King, C.A.; Lin, C.J.; Mansour, Y.; et al. Load representation for dynamic performance analysis (of power systems). *IEEE Trans. Power Syst.* **1993**, *8*, 472–482. [CrossRef]
38. Niknam, T.; Kavousifard, A.; Aghaei, J. Scenario-based multiobjective distribution feeder reconfiguration considering wind power using adaptive modified particle swarm optimisation. *IET Renew. Power Gener.* **2012**, *6*, 236–247. [CrossRef]
39. Aien, M.; Hajebrahimi, A.; Fotuhi-Firuzabad, M. A comprehensive review on uncertainty modeling techniques in power system studies. *Renew. Sustain. Energy Rev.* **2016**, *57*, 1077–1089. [CrossRef]
40. Kreishan, M.Z.; Zobaa, A.F. Optimal Allocation and Operation of Droop-Controlled Islanded Microgrids: A Review. *Energies* **2021**, *14*, 4653. [CrossRef]
41. Probability Methods Subcommittee. IEEE Reliability Test System. *IEEE Trans. Power Appar. Syst.* **1979**, *PAS-98*, 2047–2054. [CrossRef]
42. Atwa, Y.M.; El-Saadany, E.F.; Salama, M.M.A.; Seethapathy, R.; Assam, M.; Conti, S. Adequacy Evaluation of Distribution System Including Wind/Solar DG During Different Modes of Operation. *IEEE Trans. Power Syst.* **2011**, *26*, 1945–1952. [CrossRef]
43. Hajipour, E.; Bozorg, M.; Fotuhi-Firuzabad, M. Stochastic Capacity Expansion Planning of Remote Microgrids with Wind Farms and Energy Storage. *IEEE Trans. Sustain. Energy* **2015**, *6*, 491–498. [CrossRef]
44. Amjady, N.; Aghaei, J.; Shayanfar, H.A. Stochastic Multiobjective Market Clearing of Joint Energy and Reserves Auctions Ensuring Power System Security. *IEEE Trans. Power Syst.* **2009**, *24*, 1841–1854. [CrossRef]
45. Jangamshetti, S.; Rau, V. Site matching of wind turbine generators: A case study. *IEEE Trans. Energy Convers.* **1999**, *14*, 1537–1543. [CrossRef]
46. Justus, C.G. *Winds and Wind System Performance*; Franklin Institute Press: Philadelphia, PA, USA, 1978.
47. Johnson, G.L. *Wind Energy Systems*; Prentice-Hall, Inc.: Englewood Cliffs, NJ, USA, 1985.
48. Fajber, R.; Monahan, A.H.; Merryfield, W.J. At What Time of Day Do Daily Extreme Near-Surface Wind Speeds Occur? *J. Clim.* **2014**, *27*, 4226–4244. [CrossRef]
49. Mohammadi, S.; Soleymani, S.; Mozafari, B. Scenario-based stochastic operation management of MicroGrid including Wind, Photovoltaic, Micro-Turbine, Fuel Cell and Energy Storage Devices. *Int. J. Electr. Power Energy Syst.* **2014**, *54*, 525–535. [CrossRef]
50. Atwa, Y.; El-Saadany, E. Probabilistic approach for optimal allocation of wind-based distributed generation in distribution systems. *IET Renew. Power Gener.* **2011**, *5*, 79–88. [CrossRef]

51. Schlueter, M.; Yam, C.H.; Watanabe, T.; Oyama, A. Parallelization impact on many-objective optimization for space trajectory design. *Int. J. Mach. Learn. Comput.* **2016**, *6*, 9–14. [CrossRef]
52. Kreishan, M.Z.; Zobaa, A.F. Mixed-Integer Distributed Ant Colony Optimization of Dump Load Allocation with Improved Islanded Microgrid Load Flow. *Energies* **2023**, *16*, 213. [CrossRef]
53. Teng, J.-H. A direct approach for distribution system load flow solutions. *IEEE Trans. Power Deliv.* **2003**, *18*, 882–887. [CrossRef]
54. Pesaran, M.H.A.; Huy, P.D.; Ramachandaramurthy, V.K. A review of the optimal allocation of distributed generation: Objectives, constraints, methods, and algorithms. *Renew. Sustain. Energy Rev.* **2017**, *75*, 293–312. [CrossRef]
55. Gupta, Y.; Nellikkath, R.; Chatterjee, K.; Doolla, S. Volt–Var Optimization and Reconfiguration: Reducing Power Demand and Losses in a Droop-Based Microgrid. *IEEE Trans. Ind. Appl.* **2021**, *57*, 2769–2781. [CrossRef]
56. Shoeb, A.; Shahnia, F.; Shafiullah, G. A Multilayer and Event-Triggered Voltage and Frequency Management Technique for Microgrid's Central Controller Considering Operational and Sustainability Aspects. *IEEE Trans. Smart Grid* **2018**, *10*, 5136–5151. [CrossRef]
57. Manna, D.; Goswami, S.K.; Chattopadhyay, P.K. Jadavpur University Droop control for micro-grid operations including generation cost and demand side management. *CSEE J. Power Energy Syst.* **2017**, *3*, 232–242. [CrossRef]
58. Gabbar, H.A.; Zidan, A. Optimal scheduling of interconnected micro energy grids with multiple fuel options. *Sustain. Energy Grids Netw.* **2016**, *7*, 80–89. [CrossRef]
59. Ma, J.; Summers, K.; Wen, F. Joint energy and reserve market design with explicit consideration on frequency quality. *Energy Convers. Econ.* **2021**, *2*, 25–34. [CrossRef]
60. Nutkani, I.U.; Loh, P.C.; Blaabjerg, F. Cost-based droop scheme with lower generation costs for microgrids. *IET Power Electron.* **2014**, *7*, 1171–1180. [CrossRef]
61. Khaledian, A.; Ahmadian, A.; Aliakbar-Golkar, M. Optimal droop gains assignment for real-time energy management in an islanding microgrid: A two-layer techno-economic approach. *IET Gener. Transm. Distrib.* **2017**, *11*, 2292–2304. [CrossRef]
62. *IEEE Std 1547.7-2013*; IEEE Guide for Conducting Distribution Impact Studies for Distributed Resource Interconnection. IEEE: Piscataway, NJ, USA, 2014; pp. 1–137. [CrossRef]
63. Baran, M.E.; Wu, F. Optimal capacitor placement on radial distribution systems. *IEEE Trans. Power Deliv.* **1989**, *4*, 725–734. [CrossRef]
64. Abdelaziz, A.; Ali, E.; Abd-Elazim, S. Optimal sizing and locations of capacitors in radial distribution systems via flower pollination optimization algorithm and power loss index. *Eng. Sci. Technol. Int. J.* **2016**, *19*, 610–618. [CrossRef]
65. Mahfoud, R.J.; Sun, Y.; Alkayem, N.F.; Alhelou, H.H.; Siano, P.; Shafie-Khah, M. A Novel Combined Evolutionary Algorithm for Optimal Planning of Distributed Generators in Radial Distribution Systems. *Appl. Sci.* **2019**, *9*, 3394. [CrossRef]
66. Kreishan, M.Z.; Zobaa, A.F. Dump Load Allocation in Islanded Microgrid with Robust Backward\Forward Sweep and MIDACO. In Proceedings of the 57th International UPEC, Istanbul, Turkey, 30 August–2 September 2022; pp. 1–6. [CrossRef]
67. Deb, K. *Multi-Objective Optimization using Evolutionary Algorithms*; John Wiley & Sons: Hoboken, NJ, USA, 2001; Volume 16.
68. Coello, C.A.C.; Toscano-Pulido, G.T.; Lechuga, M.S. Handling multiple objectives with particle swarm optimization. *IEEE Trans. Evol. Comput.* **2004**, *8*, 256–279. [CrossRef]
69. Sierra, M.R.; Coello, C.A.C. Improving PSO-Based Multi-objective Optimization Using Crowding, Mutation and ∈-Dominance. In Proceedings of the 3rd ICEMO Conference, Guanajuato, Mexico, 9–11 March 2005; pp. 505–519. [CrossRef]
70. Deb, K.; Pratap, A.; Agarwal, S.; Meyarivan, T. A fast and elitist multiobjective genetic algorithm: NSGA-II. *IEEE Trans. Evol. Comput.* **2002**, *6*, 182–197. [CrossRef]
71. Deb, K.; Agrawal, S. A Niched-Penalty Approach for Constraint Handling in Genetic Algorithms. In Proceedings of the ICANNGA Conference, Portorož, Slovenia; 1999; pp. 235–243. [CrossRef]
72. Hansen, K. Decision-making based on energy costs: Comparing levelized cost of energy and energy system costs. *Energy Strategy Rev.* **2019**, *24*, 68–82. [CrossRef]
73. Li, Z.; Xu, Y.; Feng, X.; Wu, Q. Optimal Stochastic Deployment of Heterogeneous Energy Storage in a Residential Multienergy Microgrid with Demand-Side Management. *IEEE Trans. Ind. Inform.* **2021**, *17*, 991–1004. [CrossRef]
74. Mostafa, M.H.; Aleem, S.H.E.A.; Ali, S.G.; Ali, Z.M.; Abdelaziz, A.Y. Techno-economic assessment of energy storage systems using annualized life cycle cost of storage (LCCOS) and levelized cost of energy (LCOE) metrics. *J. Energy Storage* **2020**, *29*, 101345. [CrossRef]